Hindawi
Journal of Nanomaterials
Volume 2017, Article ID 5323164, 31 pages
https://doi.org/10.1155/2017/5323164

Review Article

Nanostructured Semiconductor Materials for Dye-Sensitized Solar Cells

Carmen Cavallo, Francesco Di Pascasio, Alessandro Latini, Matteo Bonomo, and Danilo Dini

Dipartimento di Chimica, Università degli Studi di Roma "La Sapienza", Piazzale Aldo Moro 5, 00185 Roma, Italy

Correspondence should be addressed to Alessandro Latini; alessandro.latini@uniroma1.it and Danilo Dini; danilo.dini@uniroma1.it

Received 17 May 2016; Accepted 9 October 2016; Published 4 January 2017

Academic Editor: Takuya Tsuzuki

Since O'Regan and Grätzel's first report in 1991, dye-sensitized solar cells (DSSCs) appeared immediately as a promising low-cost photovoltaic technology. In fact, though being far less efficient than conventional silicon-based photovoltaics (being the maximum, lab scale prototype reported efficiency around 13%), the simple design of the device and the absence of the strict and expensive manufacturing processes needed for conventional photovoltaics make them attractive in small-power applications especially in low-light conditions, where they outperform their silicon counterparts. Nanomaterials are at the very heart of DSSC, as the success of its design is due to the use of nanostructures at both the anode and the cathode. In this review, we present the state of the art for both *n*-type and *p*-type semiconductors used in the photoelectrodes of DSSCs, showing the evolution of the materials during the 25 years of history of this kind of devices. In the case of *p*-type semiconductors, also some other energy conversion applications are touched upon.

1. Part I: *n*-Type Semiconductors

1.1. Introduction. A dye-sensitized solar cell (DSSC) is a semiconductor-based photovoltaic device that directly converts both artificial and natural (solar) radiation into electric current. In contrast to the conventional systems, where the semiconductor assumes both the tasks of light absorption and charge carrier separation and transport, the two functions are separated in a DSSC. In a conventional DSSC, light is absorbed by a sensitizer, which is anchored to the surface of a wide band gap *n*-type semiconductor [1]. Often referred to as a Grätzel cell, this hybrid device was first reported to the scientific world in 1991 by the seminal publication of Brian O'Regan and Michael Grätzel presenting a device made of sensitized nanocrystalline TiO_2 with a power conversion efficiency of 7.1% [2]. DSSCs constitute probably the cheapest photovoltaic technology today available and their efficiency has been constantly improved in the last 25 years. The confirmed efficiency record is 11.9% [3], achieved by the Sharp company. However, it was Mathew et al. that reported the best performing DSSC in literature up to now. DSSCs fabricated utilizing $[Co(bpy)_3]^{2+/3+}$ as redox couple and the SM315 dye demonstrated panchromatic light-harvesting without the use of cosensitization, leading to a record efficiency value of 13% under one-sun illumination [4]. DSSC is an ecofriendly technology that can be used to produce electricity in a wide range of light conditions, indoors and outdoors. If one considers that dye-sensitized solar cells work properly also under low irradiation conditions, the efficiencies they reach make the technology extremely interesting with respect to conventional solar cells in such conditions. The DSSCs and their inventor received prestigious awards, including the Balzan Prize in 2009 and the 2010 Millennium Technology Prize, the most important technology prize in the world [5].

1.2. Device Structure and Operation Principles: Brief Discussion of Components and Their Role in DSSC. A simple scheme of the components and of the basic operating prinles of a

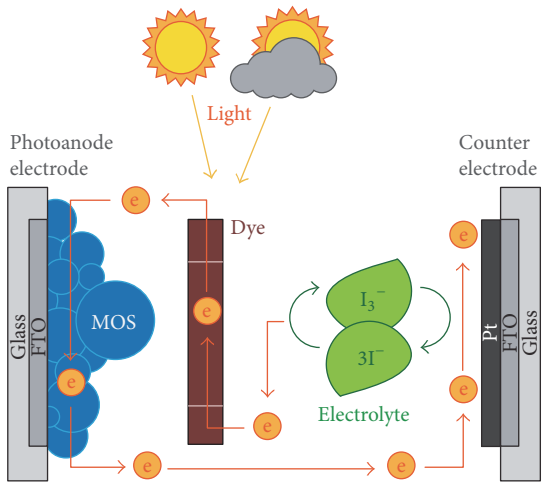

FIGURE 1: Schematic representation of a DSSC device.

DSSC is reported in Figure 1. The device is comprised of four components only:

(i) Nanostructured *n*-type semiconductor (wide band gap metal oxide) coated over transparent conducting substrate (TCO (ITO [6] or FTO [7]))

(ii) Visible-light absorber dye (several organic dye can be used, such as N3 [8], N719 [9], N749 [10] (the so-called black dye), K8 [11], K19 [12], CYC-B11 [13], and C101 [2])

(iii) Electrolyte [14, 15]

(iv) Counterelectrode (TCO coated with a platinum layer or other suitable catalyst)

In the case of *n*-type materials, current is generated when a photon absorbed by a dye molecule causes an electron injection into the conduction band of the semiconductor. The dye molecules are anchored to the surface of the semiconductor particles by a chemical bond (sensitization). In a nanostructured oxide, the semiconductor provides a large surface area for dye molecule anchoring. The photons are absorbed at the surface of the nanostructure by the dye, promoting its excitation and then the electron injection. The photogenerated electrons are injected into metal oxide and the dye is regenerated by a redox species present in the electrolyte. The electrons move through the semiconductor to a current collector and then to an external circuit. The redox mediator is regenerated at the cathode, and the process is cyclic. Each part of the device heavily determines the cost and the efficiency of DSSCs. The optimization of light absorption properties can be achieved by modifying the dye alone, while charge transport properties can be improved by the optimization of the semiconductor and of the electrolyte composition [16]. Thus, in the last years, almost all research efforts have been focused on the modification of each component for practical applications. Ye et al. [17] reported a scheme of the number of publications for sensitized solar cells. The major area of interest was represented by the fabrication of *n*-type nanostructured semiconductor photoanodes with improved architectures for high dye loading and fast electron transport. Therefore, this section of the present paper aims at bringing together the various contributions brought about by researchers to improve the efficiency of the *n*-type sensitized semiconductors for DSSCs. Moreover, the detailed discussion of the role of band gap, morphology, composition, and doping of *n*-type semiconductors for the development of efficient photoanodes will be reported. Several contributions are summarized here with the description of nanostructures (0D, 1D, 2D, 3D, and mesoporous nanostructures) and of the effect of doping of photoanodes materials (mostly TiO_2 and ZnO) on the performances of DSSCs.

1.3. Photoanode Materials for n-Type DSSC. Semiconducting nanostructured films are the main core of DSSCs photoanodes. The main issues in DSSCs are the charge recombination processes and their relatively low light-harvesting capability. The photoanode performs a dual function as both the support for the sensitizer and carrier of photogenerated electrons from the sensitizer to the external circuit [17]. The photoanode material should not absorb visible light and should have sufficiently high surface area for optimum dye adsorption.

In semiconductor terminology, the top of the valence band and the bottom of the conduction band are called the *valence band edge* and the *conduction band edge,* respectively. The energy of the conduction band edge is denoted as E_{CB}; similarly, the energy of the valence band edge is denoted as E_{VB}. The energy difference between these levels is called the *band gap* (E_g). The size of this band gap is perhaps the most important property of a semiconductor, as it influences all of the most important electronic properties of the material [18]. The conduction band edge E_{CB} of the photoanode material should match with that of the excited dye molecules. To efficiently collect the photogenerated electrons, the photoanode should have high charge carrier mobility.

Desirable properties of the material are also the ease to preparation, stability, low-cost, and environmental friendliness. These properties are the defining characteristics of an ideal photoanode [19].

1.3.1. N-Type Semiconductors. Probably it was Faraday [20] that made the first significant observation in the semiconductor science in 1833 when he discovered the negative temperature resistivity coefficient of silver sulfide [21]. Nowadays, semiconductors are defined by the unique behaviour of their electrical properties. As their name implies, semiconductors possess an electrical conductivity intermediate between conductors such as metals and insulators such as ceramics [22]. For high-density electron ensembles such a valence electrons in metals, Fermi statistic is applicable. The Fermi level, E_F (defined 0 K as the energy at which the probability of finding an electron is 1/2) can be regarded as the electrochemical potential of the electron in a particular phase (in this case, a solid). Thus, all electronic energy levels below E_F are occupied and those above E_F are likely to be empty. Electrons in semiconductor may be regarded as low-density particles ensembles such that their occupancy in the valence (VB)

and conduction bands (CB) may be approximated by the Boltzmann function [23, 24]:

$$n_e \approx N_0 \exp\left(-\frac{E_0 - E_F}{kT}\right). \quad (1)$$

Now, we come to another important distinction between metals and semiconductors in that two types of electronic carriers (*ni*, *pi*) are possible in the latter. Consider the thermal excitation of an electron from VB to CB. This gives rise to a free electron in the CB and a vacancy or hole in the VB. Thus, (1) becomes

$$n_i \approx N_c \exp\left(-\frac{E_F - E_{\mathrm{CB}}}{kT}\right),$$
$$p_i \approx N_v \exp\left(-\frac{E_{\mathrm{VB}} - E_F}{kT}\right), \quad (2)$$

where N_c and N_v are the effective density of states (in cm^{-3}) at the lower edge and top edge of CB and VB, respectively. These expressions can be combined with the recognition that $n_i = p_i$ to yield

$$n_i^2 \approx N_0 \exp\left(-\frac{E_{\mathrm{VB}} - E_{\mathrm{CB}}}{kT}\right) \approx N_0 \exp\left(-\frac{E_g}{kT}\right). \quad (3)$$

To provide a numerical sense of the situation, N_c and N_v are typically both approximately $10^{19}\ \mathrm{cm}^{-3}$ so that the constant $N_0(N_cN_v)$ in (1) is about $10^{38}\ \mathrm{cm}^{-3}$.

The latter case refers to the semiconductor in its intrinsic state with very low carrier concentrations under ambient conditions. The Fermi level, E_F, in this case lies approximately in the middle of the energy band gap [25]. This simply reflects the fact that the probability of the electron occupancy is very high in VB and very low in CB and does not imply an energy level at E_F itself that can be occupied.

In extrinsic semiconductors, the carrier concentrations are perturbed such that $n \neq p$. The analogy with the addition of an acid or base to water is quite instructive here. Consider the case when donor impurities are added to an intrinsic semiconductor. Since the intrinsic carrier concentrations are low (subparts per trillion), even additions in part per billion levels can have a profound electrical effect. This process is known as doping of the semiconductor. In this particular case, the Fermi level shifts towards the one of the bands' edges. When the donor level is within a few kT in energy from the CB edge, appreciable electron concentrations are generated by donor ionization process (at ambient temperatures) such that now $n \gg p$. This is termed *n-type* doping, and the resultant (extrinsic) semiconductor is called *n-type*. By analogy, *p-type* semiconductors have $p \gg n$. The terms minority and majority carriers now become appropriate in these cases. For a *p-type* semiconductor case, the Fermi level now lies close to VB edge. The Fermi level determines the tendency of the semiconductor to transfer charges to other phases. The movement of E_F with dopant concentration can also be rationalized via the Nernst formalism [26].

Doping can be accomplished by adding aliovalent impurities to the intrinsic semiconductor. For example, P (a group 15 or VB element) will act as a donor in Si (a group 14 or IVB element). This can be rationalized on chemical terms by noting that P need only four valence electrons for tetrahedral bonding (as in Si lattice) and the fifth electron is available for donation by each P atom. The donor density, N_D nominally is approximately $10^{17}\ \mathrm{cm}^{-3}$. Thus, assuming that $n \cong N_D$ (complete ionization at 300 K), p will be only approximately $10^3\ \mathrm{cm}^{-3}$ (recall the product $n_ip_i \sim 10^{20}\ \mathrm{cm}^{-6}$), bearing out the earlier qualitative assertion that $n \gg p$.

Impurity addition, however, is not the only doping mechanism. Nonstoichiometry in compound semiconductors such as CdTe also gives rise to *n*- or *p*-type behaviour, depending on whether Cd or Te is in slight excess, respectively. For metal oxides, doping with suitable cation/anion modifies band gap and may modulate their electrical properties. The defect chemistry in these solid chalcogenides controls their conductivity and doping in a complex manner. Excellent treatises are available on this topic and on the solid-state chemistry of semiconductors in general [27]. The distinction between metal and semiconductor electrodes is important when we consider the electrostatics across the corresponding solid-liquid interfaces [metal oxide semiconductor (MOS)/electrolyte].

1.3.2. N-Type Semiconductor-Electrolyte Interface. The electrochemical potential of electrons in a redox electrolyte is given by the Nernst expression:

$$E_{\mathrm{redox}} = E^0_{\mathrm{redox}} + \frac{RT}{nF} \ln\left[\frac{c_{\mathrm{ox}}}{c_{\mathrm{red}}}\right], \quad (4)$$

where c_{ox} and c_{red} are the concentrations of the oxidized and reduced species, respectively, in the redox couple. The parameter ($E_{\mathrm{redox}} = \mu_{e,\mathrm{redox}}$) as defined by this equation can be identified with the Fermi level ($E_{F,\mathrm{redox}}$) in the electrolyte. When a semiconductor is immersed in this redox electrolyte, the electrochemical potential (Fermi level) is disparate across the interface. Equilibration of this interface thus necessitates the flow of charge from one phase to the other and a "band bending" ensues within the semiconductor phase. For an *n*-type semiconductor (TiO_2) electrode at open circuit, the Fermi level is typically higher than the redox potential of the electrolyte, and hence electrons will be transferred from the electrode into the solution. Therefore, there is a positive charge region, and this is reflected in an upward bending of the band edges [28] (see Figure 2). Since the majority charge carrier of the semiconductor has been removed from this region, the latter is also referred to as the *depletion* layer.

1.3.3. N-Type Nanostructured Semiconductor for DSSCs. Nanostructured materials present a specific surface area significantly larger than that of the corresponding bulk materials. The nanoscale size may also affect the behaviour of electrons transport in nanostructures in view of a limit to the electron mean free path. This is called *quantum confinement effect* [29–31]. The quantum confinement effect is observed when the size of the particle is too small to be comparable to the wavelength of the electron. On the optics side, by forming photonic band gap, periodic nanostructures (known as a photonic crystals) also are shown to be special in light

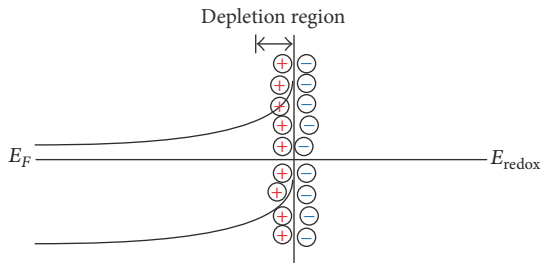

Figure 2: Band bending for *n*-type semiconductor in equilibrium with electrolyte.

manipulation and management through generating *optical confinement* or *photonic localization* [32–35]. These unique properties of nanomaterials received considerable attention and have been extensively investigated for applications in electronic, optoelectronic, photovoltaic, photocatalytic, and sensing devices [36–40]. The metal oxides in their nanoform can be synthesized under various morphologies with different shapes and sizes, thus offering the possibility for modulating their properties.

The crystallinity of the metal oxides should be high to prevent the recombination of e^- and h^+. Ohtani et al. clarified that the photocatalytic activity of TiO_2 powders strongly depends on its physical properties such as crystal structure, surface area, particle size, and surface hydroxyls [41]. In literature, a variety of preparation techniques, such as sol-gel [42], hydrothermal/solvothermal [43, 44], electrochemical anodization [45], electrospinning [46, 47], spray pyrolysis [48], and atomic layer deposition [49], have been developed and applied to obtain different morphologies in photoanode materials. Asim et al. summarized the different preparation and deposition methods, which have been used for photoanode materials of DSSCs, emphasizing their advantages and disadvantages, in order to allow a researcher to carefully choose and optimize a given method [50]. Perez-Page et al. [51] presented several methods based on templates for shape-controlled nanostructuring. A variety of nanostructured materials are produced through template-based syntheses, including zero-dimensional (nanoparticles), one-dimensional (nanowires, nanotubes, etc.), and two dimensional (nanoflakes and nanosheets) structures [51]. In 1995, Ying and Antonelli for the first time reported the synthesis of mesoporous TiO_2, which was accomplished through a modified sol-gel process involving TIP (titanium isopropoxide) as a precursor [52]. Later, various procedures have been developed for the synthesis of mesoporous materials. In 2001, Grosso et al. [53], Yun et al. [54], and Hwang et al. [55] reported syntheses of mesoporous titania films in the anatase phase. In the development of a simple and general methodology for the synthesis of highly organized mesoporous metal oxide, Sadatlu and Mozaffar proposed a novel and effective strategy [56].

1.3.4. Nanoparticles-Based Semiconductors (0D Nanostructures). A typical DSSC photoanode is composed of nanocrystalline semiconductors. Sufficient light absorption is achieved by the nanocrystalline form of the semiconductor, because a large internal surface area increases the dye concentration in the film per unit device area. Wide band gap MOSs (E_g > 3 eV) [57], such as TiO_2 [58–60], ZnO [61–67], SnO_2 [60, 68–71], and Nb_2O_5 [72–74], have been studied more or less extensively and used as photoanode materials for DSSC devices. These MOSs present good stability against photocorrosion, transparency in the major part of the solar spectrum, and good electronic properties [75–78]. Photocorrosion, which is caused by the oxidation by holes (generated through band gap excitation) of the redox species in the electrolytes, may affect the performance of the semiconductor.

TiO_2 is a low-cost, widely available, nontoxic, and biocompatible material. It has been used in health care products as well as in domestic applications such as paint pigments [16]. On the other hand, ZnO, which has a similar conduction band edge and work function compared to TiO_2, but with a higher carrier mobility than TiO_2, was considered as a promising photoanode materials for DSSCs. However, the instability of ZnO in acidic environment and formation of dye aggregates on its surface deteriorate its performances [79]. This is probably due to its acidic surface and more positive (versus NHE) conduction band edge position compared to TiO_2. Some other semiconductor materials, such as Zn_2SnO_4 [80], CeO_2 [81], WO_3 [82], $SrTiO_3$ [83], In_2O_3 [84], and $Al_{64}Cu_{25}Fe_{11}$ [85] were also studied. Alami et al. evaluated the suitability of the $Al_{64}Cu_{25}Fe_{11}$ intermetallic compound to enhance spectral solar absorption when replacing the mesoporous layer material of DSSCs. Zheng et al. [86] presented for the first time a complete study on WO_3 as photoanode material for DSSC.

The efficiency of DSSCs using these materials with a suitable redox electrolyte should be around 10–15% under one-sun irradiation. The main issues in DSSCs are charge recombination processes and their relatively low light-harvesting efficiency. As stated before, the photoanode performs a dual function as both the support for the sensitizer and carrier of photogenerated electrons from the sensitizer to external circuit [17]. In this regard, a major benefit of using nanostructured materials in DSSCs is that the resulting photoelectrode films are highly porous. Porous nanostructures offer a larger surface area for dye absorption compared to a bulk material. Among all semiconductor oxides, porous, anatase phase titanium dioxide (TiO_2) is the best and most common choice for high-efficiency DSSCs due to its low-cost, easy synthesis, nontoxicity, and biocompatibility [87]. A photoanode based on nanosized TiO_2 crystals with various geometries, such as nanoparticles [88], ordered mesostructured materials [89, 90], and one-dimensional structured materials, for example, nanorods, nanowires, and nanotubes [91, 92], has been extensively studied. Up to now, the most efficient DSSCs are based on TiO_2 nanoparticles owing to their integrated advantage in porosity, dye absorption, charge transfer, and electron transport. Moreover, electron transport in nanoparticles films suffer from trapping/detrapping processes [93]. Trapping is an important effect affecting the electron lifetime in the semiconductor, significantly reducing the electron diffusion length, L_e. In order to have a quantitative collection of electrons at the anode, condition $L_e \gg d$ should be satisfied,

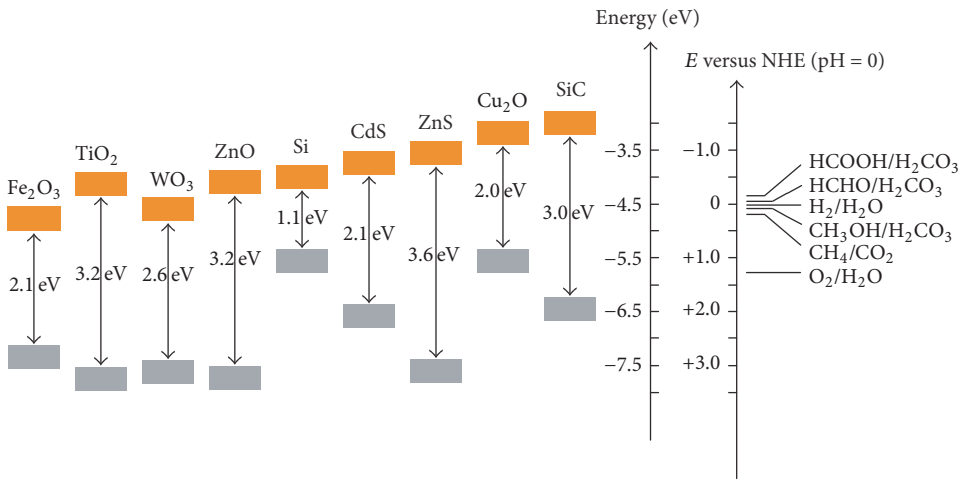

FIGURE 3: Band gap positions of several semiconductors relative to energy of some redox couples in contact with aqueous electrolyte at pH = 0 (adapted from [102]).

with d being the semiconductor film thickness. Quaranta et al. [94] showed that L_e can be increased by a given quantity of functionalized multiwalled carbon nanotubes (MWCNTs) coated by nanostructured TiO_2-anatase. Moreover, other 0D structured photoanodes were used to prevent this drawback of nanoparticles. Chen et al. [95] prepared a core-shell structure that consisted of a nanoporous TiO_2 film coated with oxides such as Nb_2O_5, ZnO, $SrTiO_3$, ZrO, Al_2O_3, and SnO_2. Moreover, Palomares et al. explained the growth of conformal metal oxide insulating overlayers (SiO_2, Al_2O_3, and ZrO_2 overlayers) on preformed nanocrystalline TiO_2 films, focusing on the ability of such insulating layers to retard interfacial recombination dynamics and thereby modulate the performance of DSSCs fabricated using these films [96].

The best performance in DSSCs has been achieved with the anatase form of TiO_2 [97, 98]. On the other hand, relatively little attention has been paid to the rutile form of TiO_2. Park and Kim [99] studied a rutile TiO_2-based DSSC [100]. Rutile is the thermodynamic stable polymorph of TiO_2 that forms when less stable polymorphs are heated at temperatures over 700°C. Therefore, the synthesis temperature of rutile TiO_2 is a potential issue for use in DSSCs since nanocrystalline morphology is hardly preserved at high temperatures. Moreover, the anatase form is preferred because of its higher band gap (3.2 eV) compared to rutile (~3 eV). High band gap energy makes anatase chemically more stable in DSSCs [101].

The bandgap values and the relative positions of the band edges of several commonly used semiconductors are shown in Figure 3 [102]. The positions of the redox levels of some of the most important couples are also shown.

The solid-state physics community has adopted the electron energy in vacuum as a reference, whereas chemists have traditionally used the normal hydrogen electrode (NHE) as energy reference. NHE lies at −4.5 eV with respect to the vacuum level. We can now relate the redox potential E_{redox} (as defined with reference to NHE) with the Fermi level E_F:

$$E_{F,\text{redox}} = -4.5\,\text{eV} - eE_{F,\text{redox}}. \quad (5)$$

Parameters related to the band gap position are the flat-band voltage (V_{FB}) and flat-band capacitance (C_{FB}). Material properties such as oxide charge, semiconductor carrier density, and the effective work function of the metal can be obtained directly from V_{FB} and C_{FB} [103, 104].

The standard method for determining the flat-band parameters is through Mott-Schottky plots.

Generally, a three-electrode single compartment configuration was adopted for capacitance analysis used to obtain Mott-Schottky plots. MOS coated on conducting glass was used as working electrode, while platinum and standard calomel electrode (SCE) were used as counter and reference electrodes, respectively. To measure the capacitance, oxide coated plates were immersed in 0.5 M Na_2SO_4 solution and the capacitances were measured as a function of the potential across the space charge layer at different frequencies [105]. Shifting of the flat-band potentials of semiconductors plays an important role in determining their photoelectrochemical properties as thin oxide films and powders. The shifting of V_{FB} can be harnessed in solar energy conversion processes in several ways. In DSSCs, the open-circuit voltage (V_{OC}) is determined by the difference between the quasi-Fermi level of electrons in the oxide film and the energy of the redox couple in the electrolyte [106]. Consequently, the shift of V_{FB} potential in the negative direction results in increase in barrier height and hence in the attainable V_{OC} of the solar cell. Similarly, the flat-band potential can be shifted negatively in order to electrolyze a redox couple that is otherwise too positive in the electrochemical series to be reactive at the illuminated semiconductor surface [107, 108]. Park and Kim also reported the relative flat-band potential and conduction band energies of some oxides such as TiO_2, ZnO, SnO_2,

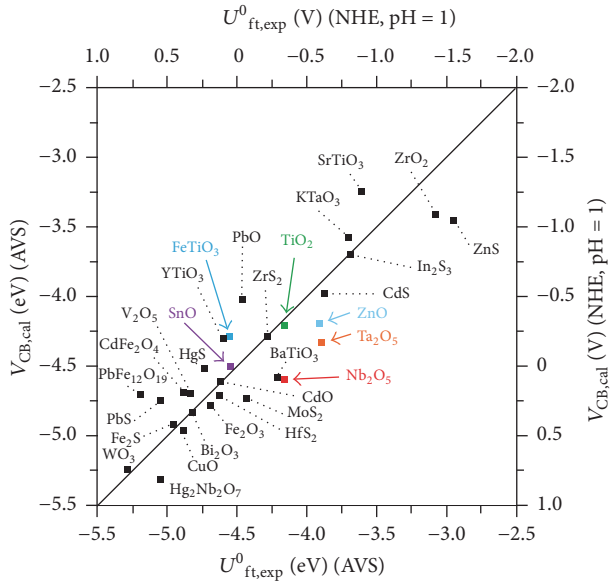

FIGURE 4: Conduction band energies and flat-band potentials of metal oxides and sulfides at pH = 1 (NHE) or vacuum level (adapted from [99]).

Nb_2O_5, $FeTiO_3$, and Ta_2O_5 and sulfides that could be used for DSSCs when considering only conduction band energy positions (adapted from [99]) (Figure 4).

1.3.5. High Ordered Nanostructures (1D Nanostructures: Nanowires, Nanotubes, etc.). A major feature that discriminates various types of nanostructures is their dimensionality. Low-dimensional nanostructures have an aligned structure that can act as a single crystal, thus facilitating the rapid electron transport in unidirectional manner, and show potentiality for obtaining high-performance devices [109]. Zhang and Cao [110] classify the nanostructures, presenting nanoparticles advantages (offer large surface area to photoelectrode film for dye absorption) and drawbacks (electron transport by trapping and detrapping processes, which may result in energy losses). In this regard, one-dimensional nanostructures such as nanowires and nanotubes provide direct pathways resulting in a much faster electron transport than in the nanoparticles films [110]. However, nanoparticles are advantageous in providing large surface area for dye absorption. Law et al. [111], for the first time in 2005, presented a comparison between a DSSC made with ZnO films made of nanoparticles and nanowires to demonstrate that one-dimensional nanostructures may provide direct pathways for electron transport in DSSCs. A high-performance nanowire photoanode must have a large surface area for dye adsorption, comparable to that of a nanoparticle film. At one-sun irradiation, the device presented an efficiency value within 1.2–1.5%. In the same year, Baxter and Adyl [112] first fabricated ZnO nanorod-based DSSC by using a hydrothermal method; they achieved an overall photoelectric conversion efficiency of 0.5%. Since then, 1D nanostructures of ZnO (nanorods and the like: Martinson et al., 2007 [113]; Schlur et al., 2013 [114]; Ameen et al., 2012 [115]; McCune et al., 2012 [116]; Guo et al., 2013 [117]) have been widely investigated as photoelectrodes for enhancing the DSSCs performances [118]. Other ZnO-based 1D structures have been investigated for photoanodes. Kim et al. studied the performance of ZnO nanofibers [119], Tan et al. constructed ZnO nanorods arrays on ITO glass [120], and Yang et al. prepared ZnO nanotips on rough Zn microtip foil [121].

ZnO-based DSSCs with delicately designed nanostructures, from irregular microrods to nanosheets with simply adjusting the dosage of capping agents in the hydrothermal synthesis process, were fabricated to study the photovoltaic performances versus morphology. In Figure 5, SEM micrographs of as-synthesized ZnO structures evolving from microrods to nanosheets are reported [122].

TiO_2 nanowires in standard DSSC configuration gave an overall conversion efficiency of 5%, which is much higher than those reported for ZnO nanowires [66, 123].

In addition, the other TiO_2 1D nanostructures gave higher efficiencies than ZnO-based ones. TiO_2 nanorods, for example, were synthesized by Chen et al. via a microemulsion electrospinning technique. The authors observed a power conversion efficiency of 8.53%, which originated from the large structure of nanorods [124].

The most studied class of one-dimensional nanostructures is that of nanotubes. The recombination rate for TiO_2 nanotubes is ~10 times lower than that of nanoparticles [125]. Their hollow structure usually gives a larger surface area than that nanowires or nanorods. Roy et al. presented a complete review of the current status of the use of TiO_2 nanotubes in Grätzel cells [126]. Since the first results in 2005 with efficiencies of 0.04%, reproducible efficiency results in the order of 4-5% have been obtained. The best morphology reported is called bamboo-type rings. This may be achieved in various ways by modifying the tube walls with porous materials (double-walled tubes). During this last year, Momeni presented a study on Cr-doped TiO_2 nanotubes [127]. The effect of chromium doping on the photovoltaic efficiency of dye-sensitized solar cells (DSSCs) with TiO_2 nanotubes prepared by an anodization procedure followed by an annealing process was investigated. He reported an interesting comparison between different doped nanotubes. In Table 1 [128–133], the obtained results are reported.

ZnO nanotubes have been also studied for application in DSSCs. The utility of high surface area Al-doped ZnO (AZO) nanotubes for DSSC application was studied by Martinson et al. [113]. Compared to similar ZnO-based DSSCs, the AZO nanotubes show superior photovoltage and fill factors with photoconversion efficiencies up to 1.6%. Xie et al. [134] prepared a novel type of coaxial TiO_2/ZnO nanotube arrays for DSSCs. The obtained efficiency is 2.8%, due to enhanced charge separation effect in this structural arrangement [134]. A smaller portion of literature is devoted to other TiO_2 one-dimensional nanostructures, for example, nanospindles [135, 136], electrospinning materials [137], and nanoembossed hollow structure (NeHS-TiO_2) [138–140]. In particular, one-dimensional hierarchical structures with hollow or porous interiors are considered promising structures due to the longitudinal pathways of the hollow or porous interior structures

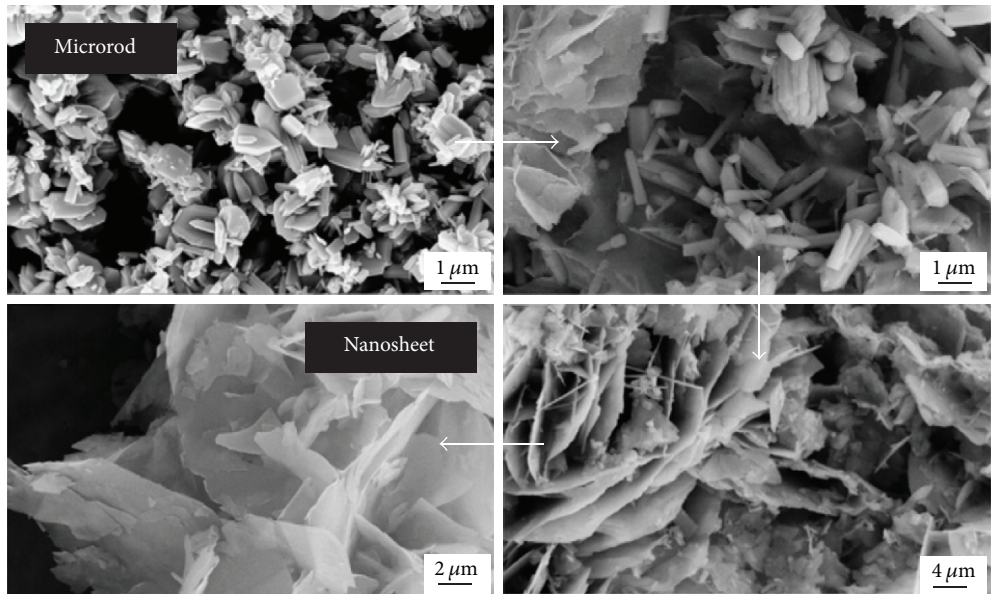

Figure 5: SEM micrographs of as-synthesized ZnO structures evolving from microrod to nanosheet with the dosage of HMTA ($(CH_2)_6N_4$) from 0 g to 1.2 g [122].

Table 1: Comparison of DSSC photovoltaic parameters of Cr-doped nanotubes with similar studies as Momemi reported [127].

Photoanodes	J_{SC}/(mA·cm^{-2})	V_{OC}/V	FF	η/%	Ref.
TNs	7.21	0.65	0.45	2.13	[128]
CdSe/TNs	6.19	0.438	0.495	1.56	[129]
P3HT/CdS/TNs	3.00	0.7	0.55	1.16	[130]
CdS/TNs	5.17	0.77	0.47	1.87	[131]
ZnS/CdSe/CdS/TNs	13.52	0.48	0.53	3.44	[132]
WO_3/TNs	6.74	0.72	0.483	2.343	[133]
Cr/TNs	10.56	0.69	0.534	3.895	[127]

and the 1D interconnected nanocrystal network that allows for efficient electron transport [141]. Wang et al. reported 1D titania with tunable structural hierarchy that exhibits about 1.3–1.5 times higher power conversion efficiency than commercial P25 as photoanode material for DSSCs [142]. Zhu et al. synthesized ZnO nanorods-nanosheets (NR-NS) hierarchical architecture [143].

1.3.6. Combination of 1D Nanostructures (2D Nanostructures). A combination of nanowires, nanotubes, and nanoparticles creates 2D nanostructures that are significant for their sufficiently high surface area available for dye loading. In the hybrid structures, the resulting photoelectrode film presents the advantages of the one-dimensional nanostructures and the exposed surface area could offer more space for dye absorption and electron conveyance. Most research was performed on the array films of ZnO and TiO_2 nanowires or TiO_2 nanotubes filled with ZnO or TiO_2 nanoparticles [144]. In Table 2, some 2D hybrid nanostructures used as photoanode of DSSC are reported [145–151].

Table 2: Photoconversion efficiencies of DSSCs based on photoanodes made of 1D nanostructures.

Type	η/%	Ref.
TiO_2 nanorod array	1.90	[145]
TiO_2 nanoflower	1.53	[145]
TiO_2 nanodisk	6.6	[146]
TiO_2 bilayer nanoribbons	5.6	[147]
TiO_2 nanoflakes	8.2	[148]
Fill-up ZnO nanowire array with nanoparticles	2.2–3.2 (0.5–0.8 ZnO nanowire only)	[149] [150]
Indium-doped ZnO (IZO) nanosheet	~7	[151]

1.3.7. 3D Nanostructures (Hierarchic Nanostructures, Composite, Multilayer, and Thin Film Materials). As we have seen until now, electron transport in nanoparticle films is via a random route with multiple trapping and detrapping events. This mechanism seriously affects the electron diffusion coefficient

and the electron collection efficiency. Moreover, small sized particles show inefficient light-scattering ability, which results in poorer light-harvesting efficiency. On the other hand, 1D and combination of 1D (2D) nanostructures attracted much attention in DSSCs owing to the improvement of the charge collection efficiency, which ascribes to a faster electron transport and slower recombination rate. However, the low surface area of 1D nanostructures hinders significant improvement of the photovoltaic performance owing to poor dye loading compared to nanoparticles. For a better balance of those three factors (surface area, light-scattering, and electron transport), bi-/trifunctional hierarchical structured materials consisting of nanoparticles/nanorods, have been widely investigated as photoanodes for DSSCs. These structures demonstrated enhanced photovoltaic performance due to their superior dye adsorption properties, light-scattering ability, and faster electron transport compared to traditional nanoparticle only based DSSCs [152]. Liao et al. in 2011 presented the effect of TiO_2 morphology on photovoltaic performance of DSSCs with particular attention on hierarchical structures [153]. Chen and Yang [154] presented a series of works in which they demonstrated the viability of new photoanode architectures in DSSCs comprising building blocks of ZnO nanoplates [155] and TiO_2 nanosplindles [135]. Recently, they presented a systematic study about DSSCs based on ZnO nanotetrapods-based photoanodes [156] and ZnO nanotetrapods/SnO_2 nanoparticles composite photoanode [157, 158]. Other authors report ZnO 3D nanostructure (e.g., caterpillar-like nanorods (η~5.2%) [116], nanodendrites (η~3.74%) [159]) based photoanodes that show significant photoconversion efficiencies for DSSC application.

Sauvage et al. [160] introduced a novel photoanode with a nanoscale structure that resembled a forest, fabricated by pulsed laser deposition (PLD) under relatively high background gas pressures. This new nanostructure, which they named "nanoforest," replaces the traditional random nanoparticle oxide network by vertically aligned bundles of TiO_2 oxide nanocrystals. Grätzel speculated earlier that a structure combining the high surface area of nanoparticles with the electron transport directionality of vertical rods would be optimal for DSSCs [16].

Another approach to the improvement of DSSC is the enhancement of the conduction band level relative to the electrolyte redox/oxidation level that would result in higher photovoltage [161]. Nb_2O_5 is an example of one such *n*-type transition metal oxide with a higher conduction band edge than TiO_2. Ghosh et al., for the first time, reported the fabrication of a Nb_2O_5-based photoanode with a nanoforest structure and the results of investigations of the photovoltaic properties of this material under a variety of key growth parameters (layer thickness, background gas pressure, and composition) [73].

Other efficient TiO_2 3D nanostructures producing good efficiency values are branching nanorods (η~7.17%) [162], dendritic hollow structures (η~7.16%) [163], bridge nanotubes (η~6.17%) [164], and so forth. Photoanodes made of two or more materials have attracted attention due to the obvious advantages of combining different materials. Yan et al. [165] combined the high electron transport rate of ZnO and the high electron injection efficiency of TiO_2 with Ru-based dyes. Huu et al. [166] presented a hierarchical photoanode comprising a SnO_2 nanoparticle underlayer and a ZnO nanorod overlayer and its photovoltaic performance was compared to photoanodes consisting of SnO_2 nanoparticles only and ZnO nanorods only.

Satapathi et al. presented a DSSC fabricated using photoanodes made from graphene-TiO_2 nanocomposites [167]. The relationship between the size of graphene sheet and the cell performance was explored. It was concluded that the cells loaded with the smaller graphene sheets yielded larger enhancement. The maximum efficiency was obtained by 184 nm sheets with η = 6.62%.

Also composite TiO_2 anatase materials with $CaTiO_3$ [168] and $BaTiO_3$ [169, 170] have been applied to electrodes for DSSCs. Among perovskite-type compound, $BaTiO_3$ is a *n*-type semiconductor with band gap energy of 3.3 eV. Such band gap value may increase the open-circuit voltage of a DSSC as Suzuki and Kijima reported in 2005 [171].

Manoharan and Venkatachalam investigated the photoelectrochemical performances of DSSCs based on aluminum doped titanium dioxide (Al-TiO_2) nanoparticles/nanowires (TNPWs) composite photoanode layers, with different electrolytes. The maximum obtained efficiency is 7.26% [172].

An efficiency value of 3.44% has been reported by Song et al. [173] using as double scattering layer a ZnO film consisting of ZnO monodisperse light-scattering layer and a submicrometer-sized plate-like ZnO film as overlayer in the photoanode of a DSSC. Ghanbari Niaki et al. presented a new strategy for improving the efficiency of TiO_2 DSSCs by design of a new double-layer film doped with Zn ions, with various morphologies [174].

1.3.8. Mesoporous Structures (3D Oxide Aggregate Nanostructures). Among 3D nanostructures, mesoporous MOS-based materials (in particular titania-based) with a crystalline framework, high specific surface area and tunable pore size have received significant attention for energy conversion applications. Several morphologies, such as mesoporous TiO_2 films [175], beads [176], monoliths [177], and networks [178], with controlled porosity have been prepared via different synthetic strategies. The most interesting are monodisperse TiO_2 beads with a submicrometric-sized diameter. Chen et al. [179] reported the synthesis of monodisperse mesoporous anatase titania beads with high surface area and tunable pore size and grain diameter via a combination of sol-gel and solvothermal processes in presence of hexadecylamine (HDA) as a structure-directing agent. In this way, they enhanced the light-harvesting capability of TiO_2 electrode without sacrificing the accessible surface for dye loading. These mesoporous TiO_2 beads have a diameter of less than 1 μm and are composed of anatase TiO_2 nanocrystals. The beads have been used in the preparation of photoanodes for DSSCs and an improved efficiency was observed when compared to analogous cells prepared using standard Degussa P25 TiO_2 photoanodes of similar thickness. An overall light conversion efficiency of 7.20% (open-circuit voltage (Voc) 777 mV, short-circuit current density (I_{SC})

12.79 mA cm^{-2}, and fill factor (FF) 0.72) was achieved using the mesoporous TiO_2 bead electrodes [180]. The substantial improvement of J_{SC} and η for the hierarchical sphere-based DSSC when compared to other nanostructure-based DSSCs is mainly due to the larger dye loading, higher light-scattering ability, faster charge transport, and longer electron lifetime [181, 182]. Submicrometric mesoporous TiO_2 beads are also used to form a scattering layer on top of a transparent, 6 mm thick, nanocrystalline TiO_2 film. Later, Sauvage et al. presented DSSCs with photoanodes made of mesoporous TiO_2 beads that achieved a power conversion efficiency over 10% [183]. Kim et al. [184] reported a two-step method for the synthesis of TiO_2 aggregates which first produced TiO_2 spheres via a controlled hydrolysis and then etched the spheres under hydrothermal conditions. These aggregates, applied to DSSCs, yielded an efficiency as high as 10.5%.

In addition, ZnO spheres were used to enhance the performances of ZnO-based DSSCs. These later were synthesized by hydrolysis of a zinc salt in polyol medium [185]. A significant difference in the conversion efficiency values (2.4% and 5.4% for ZnO nanoparticles and aggregates, resp.) has been verified. The explanation of this difference is based on the consideration that ZnO is not stable in an acidic dye solution and the formation of a Zn^{2+}/dye complex on the surface of ZnO may seriously hinder the electron injection process from the dye molecules to the semiconductor [186]. In the case of film made of ZnO nanoparticles, the formation of complex on the film surface would block the pores and result in an incomplete infiltration of dye molecules [187]. However, the situation is quite different in the case of aggregates. Due to the existence of large pores among the submicron-sized aggregates, the dye penetration can be accomplished in a very short time (e.g., 30 min) prior to the formation of the complex layer [185, 188]. Other mesoporous structures have been investigated for DSSCs applications. The use of preformed mesoporous solid as hard templates allows for the preparation of novel mesostructures of TiO_2 with high crystallinity. Moreover, hard templates can provide an excellent support and confinement framework to prevent collapse of mesoporous structures, thus allowing for high crystallinity. All these characteristics are found in mesoporous single crystals (MSC) of anatase, which were first prepared by Crossland et al. [189]. The MSC anatase displays higher conductivity and electron mobility than those of conventionally used nanoparticles. In solid-state DSSCs they obtained a power conversion efficiency of 7.2%. Latini et al. [190] used MSC as photoanode for conventional DSSCs in a comparison between hard and soft template-based materials. Five different anatase phase mesoporous titanias were used as photoanodes in DSSCs: two materials were synthesized by using silica nanospheres (hard template) and the other three using two different organic polymeric templating agents, P123 and Brij 58 (soft template). Unexpectedly, MSCs are the least suitable for application in DSSCs because of their low specific surface area. Finally, Zhang et al. developed a simple surfactant-sulfuric acid carbonization method to synthesize ultrastable ordered mesoporous titania with high crystallinity [191].

1.3.9. Doping and Codoping Effect on Nanocrystalline and Mesoporous Structures. In addition to the optimization of the oxide nanostructure, the combined use of different metal oxides and/or the use of doped materials with higher conduction band energies should, in principle, allow further improvement of DSSCs performances. In metal oxides, the doping with suitable cation/anion modifies the band gap and may modulate their electrical proprieties. The properties of titania, including anatase to rutile phase transition as well as the photoactivity, greatly depend on the presence of dopants, that is, cations [192] and anions [193] and impurities, as well as on the crystallinity [194, 195], grain size, surface area, and so on, in addition to the presence of such substances as amorphous silica at the interfaces and/or grain boundaries. All these properties have a profound influence on the mass transfer rate, diffusion, and crystallite growth of titania in composite nanoparticles [196].

The ionic radii of niobium Nb^{5+}, aluminum Al^{3+}, gallium Ga^{3+}, yttrium Y^{3+}, and scandium Sc^{3+} are quite close to that of titanium Ti^{4+}. Solid solutions of these cations in titania have been prepared and characterized [197]. For example, Chandiran et al. studied the effect of Ga^{3+} and Y^{3+} in mesoporous anatase and of Nb^{5+} in nanocrystalline anatase for DSSCs photoanodes [198, 199]. Latini et al. [105] reported the beneficial effect on the performances of DSSCs of Sc^{3+} doping of mesoporous anatase beads. At 0.2% of Sc atoms, a maximum efficiency of 9.6% was obtained, which was found to be 6.7% greater than the efficiency of DSSCs with pure anatase. Li et al. [200] reported a DSSC based on TiO_2 photoanode that was modified by the Al-doped TiO_2 layers using the chemical bath deposition method. The Al-doped TiO_2 layer improved the photocurrent density. The effect of a codopant M (M = Ga, Al, Sc) on the formation, crystallite growth, optical band gap, photocatalytic activity, and phase stability of anatase-type TiO_2 solid solutions ($Ti_{1-2X}Nb_XM_XO_2$) containing the same amount of dopant Nb that were directly formed as nanoparticles under mild hydrothermal conditions at 180°C for 5 h, was investigated by Hirano and Ito [201]. The effect of lanthanum ions (La^{3+}) on charge trapping in dye-sensitized solar cell (DSSC) photoanodes has been investigated with doped and surface-treated TiO_2 nanoparticles [202]. Including those mentioned before, transition metal dopants in general could extend the photoresponse in the visible-light region. This is due to low energy photon excitations of the corresponding metal oxide clusters with smaller band gap and partially from the excitations of the introduced localized states in the band gap of doped TiO_2 [203].

On the other hand, nonmetal dopants (N, C, B, S, P, etc.) can exist as isolated atoms rather than clusters, which have greater potential for realizing visible-light photoactivity [204]. In anion doped TiO_2, the formation in the oxide phase of new defect levels slightly above the valence band generally causes the red shift of absorption spectrum [205–209]. Pan et al., for example, presented the enhanced efficiency of DSSCs by trace amount Ca-doping of TiO_2 photoelectrodes. The best photovoltaic performance was obtained from 50 ppm Ca-doping with a conversion efficiency of 7.45% [210]. In Table 3

Table 3: Efficiency of the DSSCs based on differently doped TiO_2 photoanodes.

Doped-TiO_2	η/%	Ref.
B	6.1	[211]
Ce	7.65	[212]
Cr	8.4	[213]
Mg	1.2	[214]
N	6.25	[215]
Nb	7.41, 7.8, 8.7	[216–218]
Sb	8.13	[219]
Sn	8.31	[220]
Tm/Yb	7.5	[221]
Ta	7.1	[222]
W	9.10, 7.42	[103, 223]

Table 4: Efficiency of the DSSCs with doped ZnO as photoanode.

Doped-ZnO	η/%	Ref.
Al	0.28, 0.964	[225, 226]
Ga	4.01	[227]
I	4.5	[228]
K	0.012	[229]
Mg	4.19, 4.11	[230, 231]
N	5	[232]

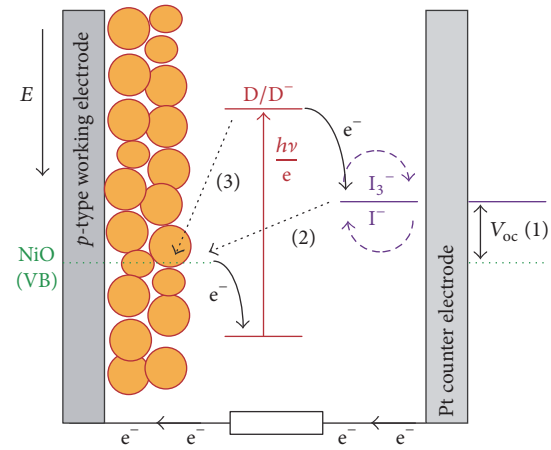

Figure 6: Diagram of the electrical potential E levels involved in the process of photoactivated electron transfer (et) at the basis of the operation of a p-DSC. The separation evidenced by the double arrow (1) represents the open-circuit voltage V_{OC} of the p-DSC. The latter parameter is determined by the difference between the Nernst level of the redox couple (I_3^-/I^-, in the given example) and the Fermi level of the p-type semiconducting electrode (NiO in the reported example). Bent full arrows represent the dye-mediated et from the p-type cathode to the oxidized form of the redox couple. The et process is catalysed by the dye-sensitizer D through the absorption of light with frequency ν. Dotted arrows (2) and (3) describe two processes of electronic recombination following the separation of charge induced by light absorption.

[211–223], some useful dopants for anatase TiO_2 have been grouped together as well as their respective photoconversion efficiencies as reported in literature.

The amount of papers dedicated to systematic studies of the effect of heteroatoms and their concentration in the anatase lattice on the performances of DSSCs are far less numerous. Cavallo et al. [224] have undertaken a systematic work of synthesis, characterization, and test of DSSC photoanodes containing mesoporous anatase bead doped with RE (rare earth) cations (Nd, Sm, Gd, Er, and Yb). The maximum efficiency has been obtained for the sample containing 0.2% Er metal atoms (8.7%).

Similarly, papers dealing with doping of ZnO with different cations and anions are also present in literature, as reported in Table 4 [225–232].

2. Part II: p-Type Semiconductors

2.1. Introduction. In the recent past, there has been a crescent interest towards the development and the realization of solar radiation conversion devices in which an electrochemical process of reduction is photoactivated via the absorption of light by a cathode either in the pristine [233–237] or in a modified/sensitized state [238–264]. These devices are photoelectrochemical cells (PECs) [40, 87] with photoactive cathodes consisting of p-type semiconducting materials and include p-type dye-sensitized solar cells (p-DSCs) (Figure 6) [242, 243, 247, 248, 264] and tandem DSCs (t-DSCs) (Figure 7) [265–269] cells of photoelectrolysis for nonfossil fuels production, namely, molecular H_2 in the process of water splitting (Figure 8) [270–281] and for carbon dioxide redox reduction (Figure 9) [282–313]. The initial charge separation produced as a consequence of light absorption [312, 313] can occur either directly on the p-type semiconductor (Figure 9) or on the electrically connected sensitizer which accomplishes successively the transfer of charge according to the vectoriality imparted by the relative positions of the energy levels of the electronic states involved and by the kinetics of the possible redox reactions (Figures 6–8).

Several requirements of thermodynamic as well as kinetics character must be fulfilled in order to realize an efficient process of photoconversion into the desired product. The latter can be the electrical power as in case of the p-DSCs [314] and t-DSCs [268] (Figures 6 and 7) and fuels/chemicals in case of the photoelectrolytic cells based on the working principles schematized in Figures 8 and 9. The most crucial aspect generally limiting the performance of radiation conversion devices is the one related to the effectiveness of charge separation. This is because the separation of charge, once effectuated, can either evolve (a) to the displacement of the charges towards the sites/reactants for the realization of the desired redox transformations (reductions in the present context) or (b) lead to the occurrence of unwanted charge recombination/trapping phenomena depending on the relative rates of processes (a) and (b) and the chemical-physical features of the various interfaces on which the events of charge separation take place [315–317]. For this reason is fundamental to envisage photoconversion devices with rapid mechanisms of photogenerated charge displacement

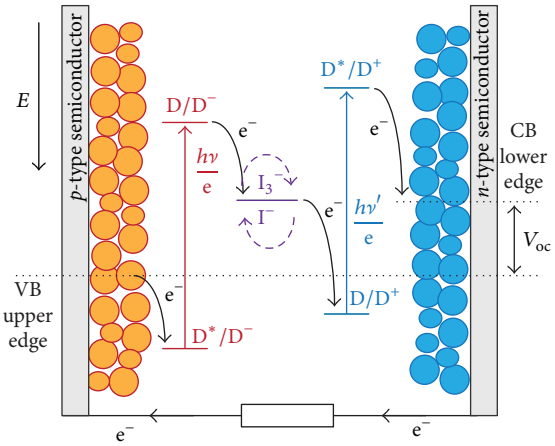

FIGURE 7: Diagram of the electrical potential E levels involved in the process of photoactivated electron transfer (et) at the basis of the operation of a t-DSC. The separation evidenced by the double arrow (1) represents the open-circuit voltage V_{OC} of the t-DSC. The latter parameter is determined by the difference between the Fermi levels of p-type cathode and n-type anode. Bent full arrows represent the dye-mediated et processes from the photoelectrodes to the corresponding forms of the redox couple (I_3^-/I^-, in the given example). The et processes are catalysed by the dye-sensitizers D and D with complementary light absorption properties.

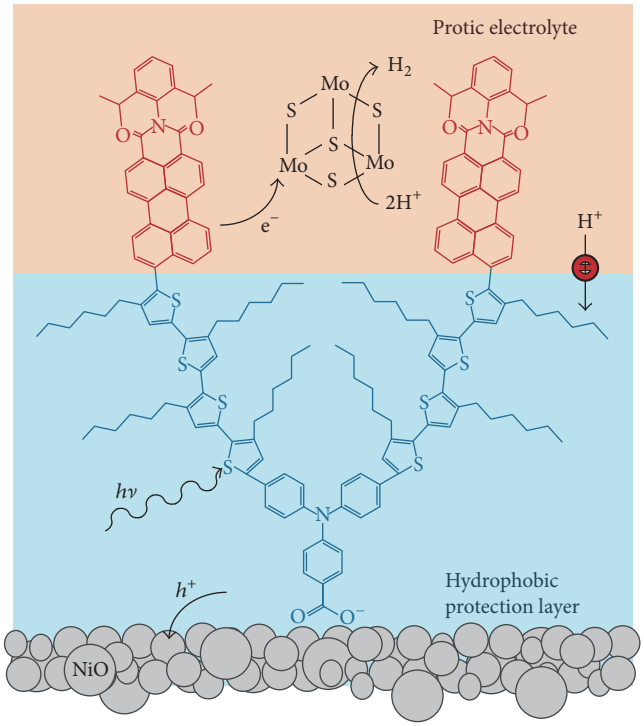

FIGURE 8: Depiction of the mechanism of photoactivated et from p-type NiO to H^+ mediated by the multifunctional dye-sensitizer PMI-4T-TPA for the production of H_2 fuel. The organic dye is immobilized onto NiO surface through the carboxylic group (in blue). The dye-sensitizer acts as electron donor (through the PMI moiety, in red) towards the molecular cocatalyst Mo_3S_4 and behaves as electron acceptor towards NiO. The hydrophobic hexyl groups (in blue) exert a blocking effect against the direct discharge of H^+ onto bare NiO cathode, adapted from [280].

within the semiconductor [318]. A relatively recent example of that has been the invention of the DSC by Grätzel [2]. The latter represents a photoconversion device in which the electrons photoinjected at a sensitized photoanode of TiO_2 in the rutile form [319] are swiftly drifted to the metallic cathode for the occurrence of a fast interfacial *et* from the cathode to the anode-generated oxidized form of a redox couple. Fundamentally, this successful result is based on very fast charge transport within the photoactive semiconducting electrode. This would prevent recombination between the photocharge generated at the surface of the light-absorbing semiconducting electrode and the redox species in the electrolyte initially oxidized/reduced by the photoinjected charge [320]. The most recent advancements in the design and realization of PECs of p-type have been achieved when the photoelectroactive p-type semiconductors had nanostructured features (Figure 10) [238, 268, 321–327]. This is motivated by the fact that a nanostructured surface increases enormously the effective area of contact for the interfaces created by the nanostructured semiconducting material with respect to the same system possessing a compact morphology. This difference improves the kinetics of those electrochemical processes occurring at an extended interface in favour to the nanostructured version [314].

Another important motive of interest in adopting nanostructured semiconductor electrodes resides in the possibility of modifying the optical properties of the pristine system through sensitization with very large amounts of dye-sensitizers anchored per unit surface [328, 329]. These colouring additives sometime represent the sole actual light-harvesting species in case the semiconductor has a wide band gap with respect to the energy of the luminous radiation [330]. On the other hand, the main concern that might arise by the utilization of nanostructured semiconductors regards the delineation of an opportune pattern of energy bands (or a set of discrete energy levels), which still allows the electrical connection through the nanostructured semiconductor [331, 332]. In fact, a nanostructured semiconductor represents a system characterized by not having an internal electric field because of the inexistence of a charge depletion layer [233–235]. In this type of semiconductors, the typically discontinuous pattern of frontier energy levels is also associated with electronic states delocalized disorderly at a variable extent [236]. Consequently, the latter feature imposes a charge transport mechanism of variable range hopping between localized states [237–340], through which the displacement of charge is originated by diffusion [341–345].

In this review, we will report the most recent developments and progress achieved with PECs having photoactive cathodes (vide supra). Despite the fast advancement of the technology of perovskite solar cells [346–380], in the present contribution, this type of device will be not reviewed since the photocurrent generated in perovskite based photoconversion devices is not associated with the primary event of photostimulated redox reactions but is rather a consequence of a

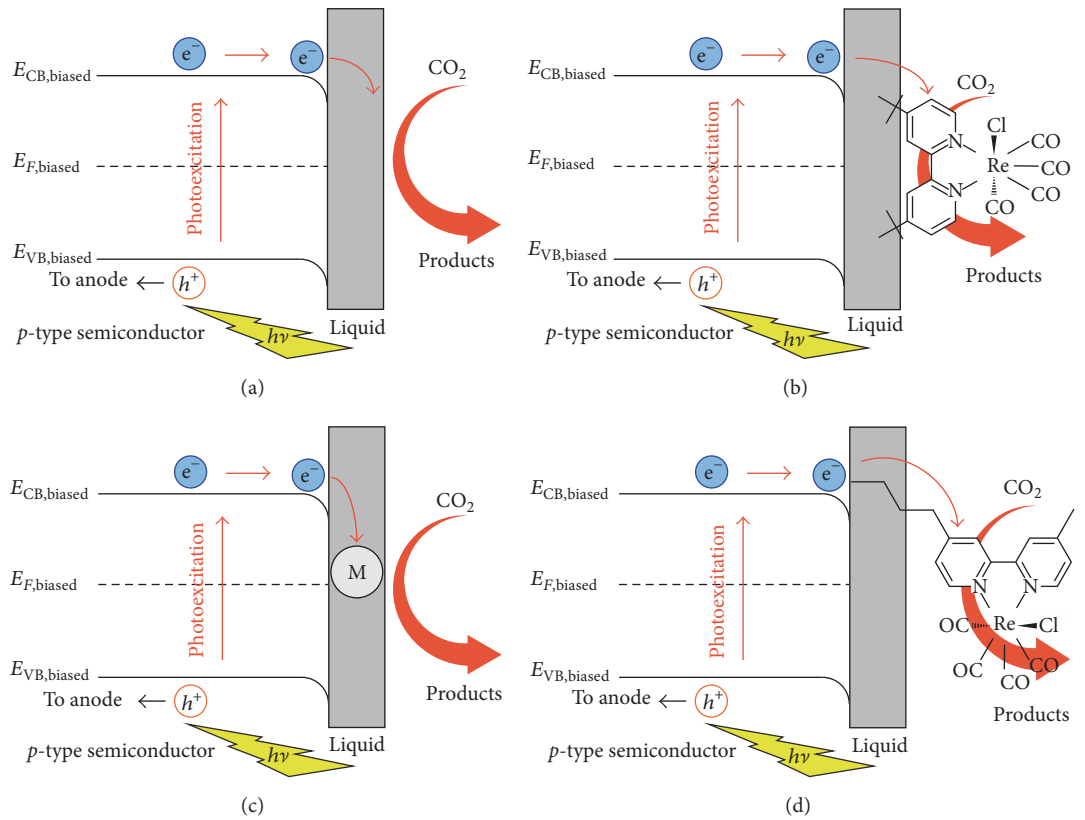

FIGURE 9: Mechanisms of photoactivated CO_2 reduction on a *p*-type semiconductor electrode: (a) heterogeneous photoelectrocatalysis occurring directly at the semiconductor electrode; (b) homogeneous catalysis mediated by a molecular catalyst in the electrolyte; (c) heterogeneous photoelectrocatalysis directly on a metal-decorated semiconductor electrode; (d) heterogeneous catalysis mediated by a molecular catalyst anchored on the semiconductor electrode. In all four examples, photoexcitation occurs at the semiconducting cathode. E_{VB}, E_{CB}, and E_F indicate the upper edge of the semiconductor valence band (VB), the lower edge of the semiconductor conduction band (CB), and the Fermi level of the *p*-type semiconductor, respectively. The illuminated electrode is reverse biased in these four examples, adapted from [282].

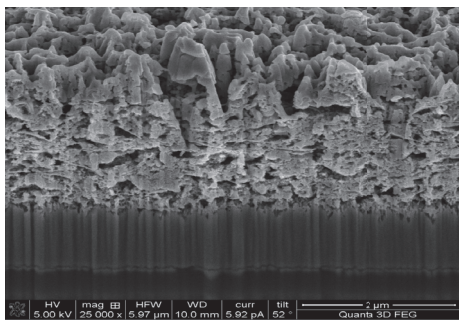

FIGURE 10: Image of the cross section of a nanostructured cathode made of nickel oxide. The picture has been obtained with the dual beam focused ion beam-scanning electron microscope (FIB-SEM), adapted from [314].

light-driven process of charge separation at a p-i-n junction. As such, it does not introduce any redox states variations in the conducting materials during ordinary operative conditions of perovskite systems [381–383].

2.2. Devices for the Conversion of the Electromagnetic Radiation into Electrical Power with Photoelectroactive p-Type Semiconductors: Analysis of Performances Recently Reported in the Literature

2.2.1. DSCs of p-Type and t-Type. One of the first studies on sensitized *p*-type semiconductors with nanostructured features for DSCs of *p*-type was reported in 2000 [268]. In this seminal work, nanoporous nickel oxide (NiO) prepared via sol-gel was employed as cathode, while erythrosine B was the dye-sensitizer. This prototypical *p*-DSC displayed a photovoltage of about 80 mV and a photocurrent density of *ca.* 0.2 mA cm^{-2}, the photocurrent being originated by the associated photoinjection of mobile holes in the VB of NiO after photoexcitation of the chemisorbed colorant (Figure 6). Despite the low overall efficiency (less than 0.1%), these results represented in principle a quite remarkable step forward especially in comparison with the modest performance of one of the first *p*-DSCs that utilized a semiconducting photocathode with compact morphology [330]. Anyhow, when compared to the analogous *n*-type counterparts,

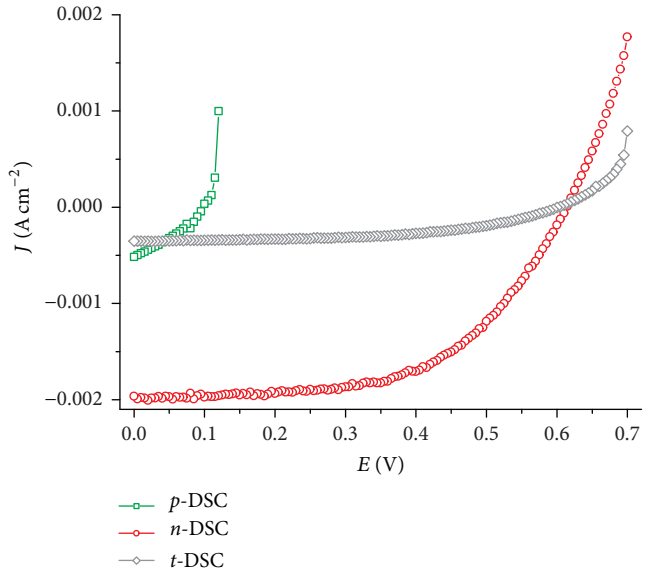

Figure 11: JV curves of a p-DSC with NiO cathode and of an n-DSC with TiO_2 anode and the corresponding t-DSC obtained upon combination of the p-DSC photocathode with the n-DSC photoanode. Anode and cathode sensitizers were N-719 and Fast Green, respectively. Redox shuttle: I_3^-/I^-. The illumination of the t-DSC with sun simulator having AM 1.5 was first directed to the side of the photoanode, adapted from [235].

p-DSCs show their relative limits especially in terms of overall efficiencies since the most performing p-DSCs reach at most 1-2% of overall conversion efficiency [384, 385], whereas there is a constant upgrade of efficiency records with n-DSCs that reach values in the broad range of 10–15% [4, 386–388]. What mainly motivates the research on p-type photoelectrochemical devices is the realization of t-DSCs (Figure 7) [265–269], which possess both electrodes with photoactive features due to their sensitization with colorants having complementary absorption properties [235].

Such a tandem configuration would allow the achievement of larger open-circuit photovoltages with respect to the corresponding DSCs having single photoactive electrodes (Figure 11), but the gain in photopotential is obtained at expenses of current density and fill factor, that are both controlled by the less performing photoactive electrode (typically the nanoporous photocathode) [235, 265–269]. The expected improvement of the overall photoelectrochemical performance in t-DSC [389] in comparison to the DSC configurations with single photoactive electrode is possible only when n- and p-type devices generate separately photocurrents and reach FFs with comparable values, the sensitizing agents of cathode and anode being complementary in terms of optical absorption (Figure 12). The present work updates the most recent achievements in the fields, which were not covered by the works of Daeneke et al. on the general limits of p-DSCs [242] and of Dini et al. [237, 241] about the influence of photocathode nature and preparation method on the relative photoelectrochemical properties in the corresponding p-DSCs. Table 5 presents the most recent achievements obtained in the best performing p-DSCs when the redox shuttle was the couple I_3^-/I^-. The comparison of the p-DSCs regards PECs differing for the structure of the dye-sensitizer [238, 239, 265, 266, 314, 327, 390–393] (Figure 12) and the nature of the nanostructured p-type photocathode [394–398].

As recognized in precedence [242], the main drawback of a p-DSC is the attainment of relatively low fill factors, which generally never exceed 40% in the most efficient configurations (i.e., with $\eta > 0.14$, Table 5) [238, 239, 265, 266, 327, 392] when the redox couple I_3^-/I^- is present. Upon adoption of a redox mediator other than the one based on iodide, the p-DSCs display performances with considerably ameliorated characteristics (Table 6) [240, 384, 399–408]. These facts would indicate that the main routes of photocathode optimization and refinement of dye-sensitizer design (Figure 13) must be necessarily accompanied by a systematic research on the selection and eventually the definition of new redox mediators in order to improve the performance of p-DSCs.

Closely related to the progress of p-DSC is the one of t-DSC with electrodes both nanostructured and opportunely sensitized [235, 265–269, 399, 409]. In terms of performance, the t-DSC represents a device still in its infancy, which strongly needs of a further stage of evolution for reaching and eventually surpassing the performances of the corresponding n-DSCs in accordance with the predictions of thermodynamics [389]. Table 7 presents the list of the parameters characterizing the performance of the t-DSCs reported so far.

3. Conclusions

The use of n-type semiconductors as photoanodes and p-type semiconductors as photoactive cathodes of p- and t-DSCs has been reviewed. Concerning the n-type semiconductor,

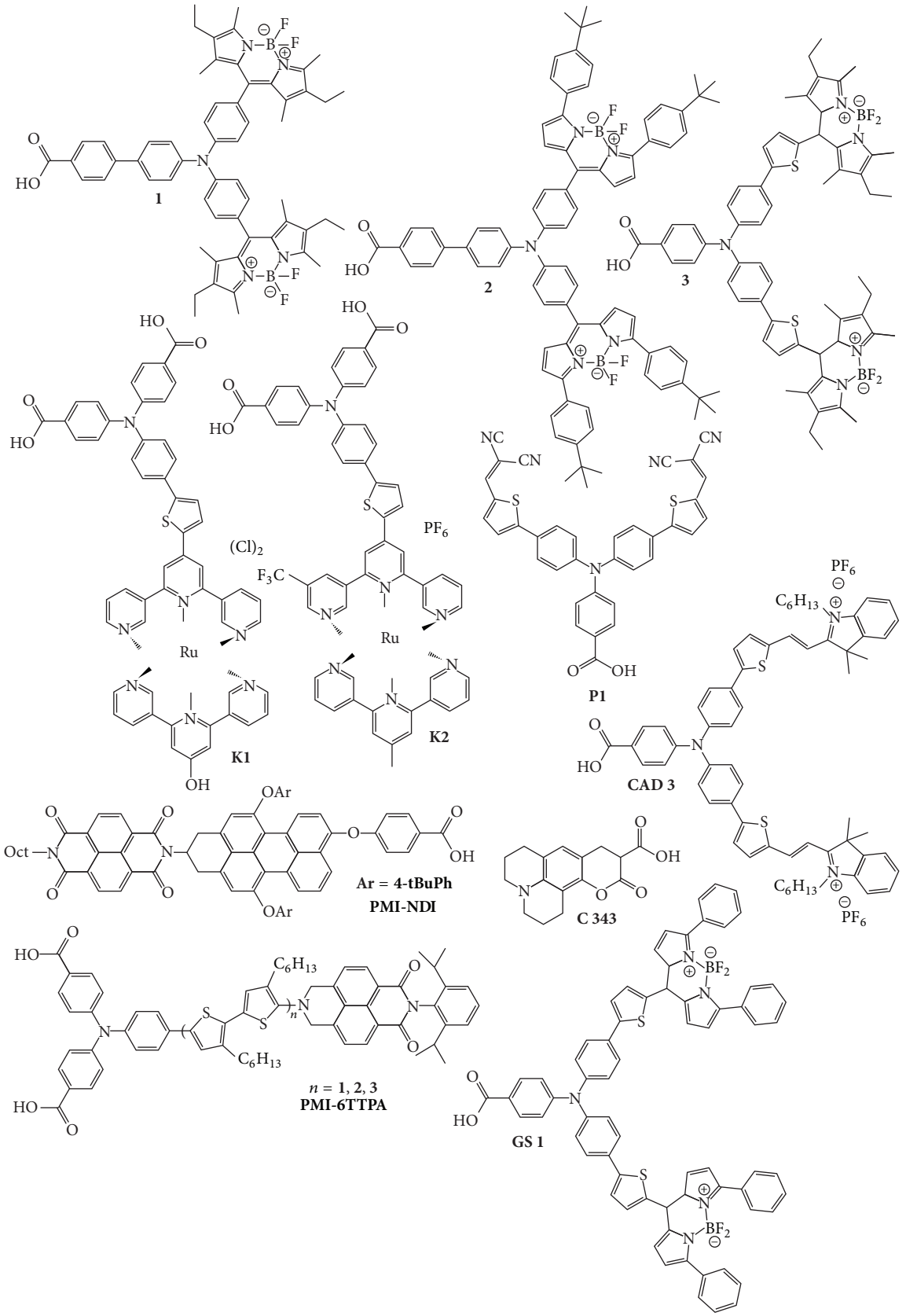

Figure 12: Structures of the most efficient dye-sensitizers insofar utilized in *p*-DSCs.

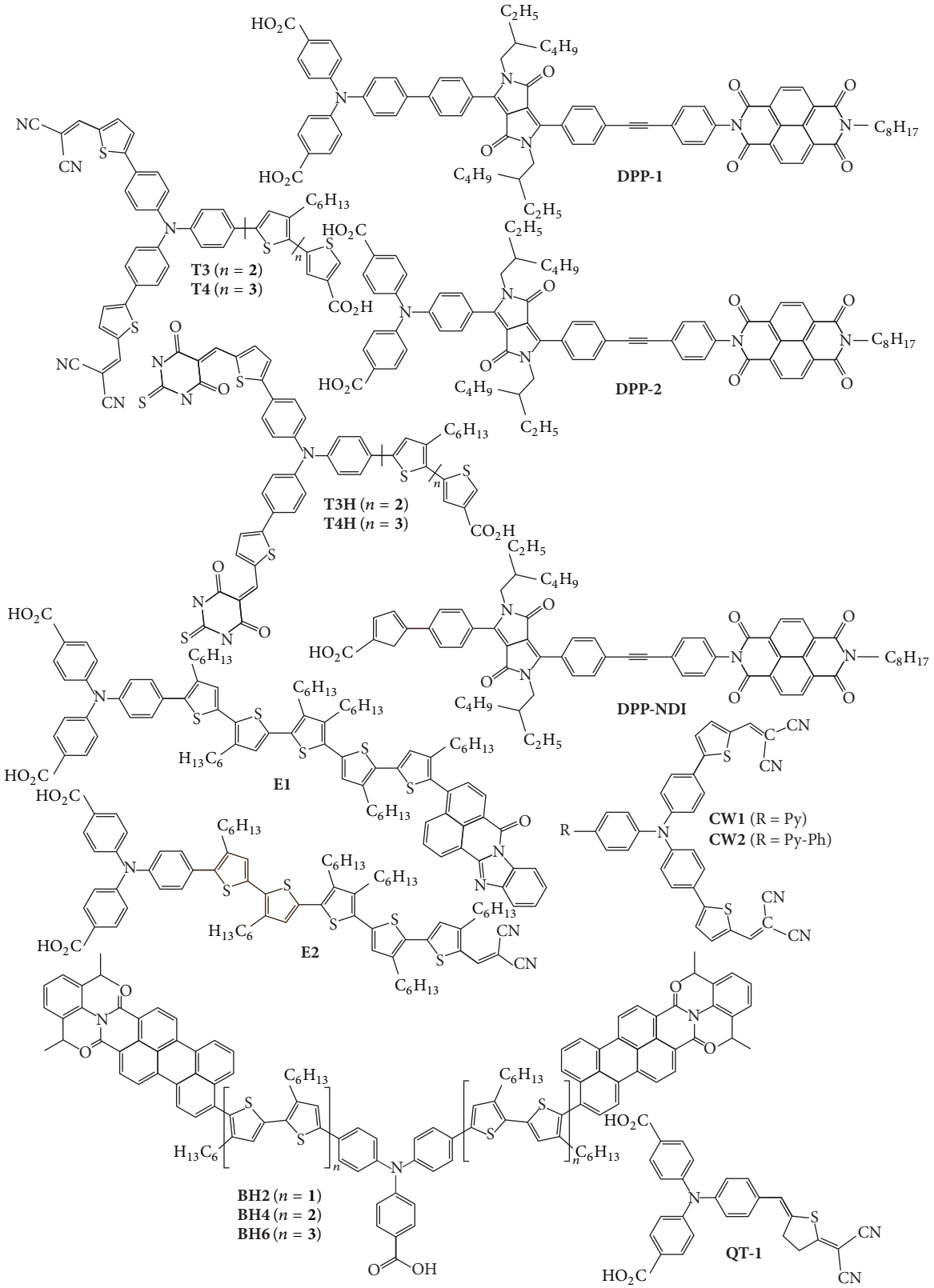

Figure 13: Structures of newly synthesized dye-sensitizers for NiO based p-DSCs with $Co^{2+/3+}$ and I_3^-/I^- redox shuttles.

Table 5: *p*-DSC parameters for devices having different nanostructured photocathodes and dye-sensitizers (Figure 8). Redox shuttle: I_3^-/I^-.

Cathode	Sensitizer	η/%	V_{OC}/mV	j_{SC}/mA cm^{-2}	FF/%	Ref.
NiO-RDS	P1	0.121	125	−2.84	33.7	[314]
NiO-CS	P1	0.110	128	−2.42	35.2	[314]
NiO sol-gel	P1	0.150	84	−5.48	34.0	[238]
NiO sol-gel	GS1	0.200	106	−5.87	31.0	[265]
NiO sol-gel	CAD1	0.250	101	−8.21	31.0	[265]
NiO sol-gel	K1	0.090	96	−2.91	32.0	[390]
NiO sol-gel	K2	0.070	93	−1.96	39.0	[390]
NiO sol-gel	**1**	0.060	97	−1.60	38.0	[239]
NiO sol-gel	**2**	0.140	109	−3.70	35.0	[239]
NiO sol-gel	**3**	0.050	95	−1.58	35.0	[239]
NiO sol-gel	**3**	0.080	79	−3.15	31.0	[391]
NiO[1]	PMI-6TTPA	0.460	208	−6.36	34.0	[321]
NiO[2]	PMI-6TTPA	0.410	218	−5.35	35.0	[266]
NiO[3]	PMI-6TTPA	0.400	292	−3.30	41.0	[392]
$CuAlO_2$	PMI-6TTPA	0.040	333	−0.30	42.0	[394]
NiO sol-gel	PMI-NDI	0.073	120	−1.76	34.5	[393]
$CuGaO_2$	PMI-NDI	0.023	187	−0.29	41.0	[395]
$CuCrO_2$	C343	0.014	145	−0.24	39.8	[396]
K_xZnO	C343	0.012	82	−0.41	35.8	[229]

RDS: rapid discharge sintering; CS: conventional sintering; 1: microballs; 2: nanoparticles; 3: nanorods.

a substantial performance improvement has been obtained by optimizing the dimensions of the particles that can be achieved by tailoring the synthesis conditions. The role of band gap, morphology, composition, and doping of *n*-type semiconductors for the development of efficient photoanodes has been reported. Several contributions were summarized here with the description of nanostructures (0D, 1D, 2D, 3D, and mesoporous nanostructures) and of the effect of doping of photoanodes materials (mostly TiO_2 and ZnO) on the performances of DSSCs. The maximum photoconversion efficiency (13–15%) is reported using titania-based photoanodes. About photocathodes, we have posed our attention towards the most recent developments on *p*-type semiconductors having nanostructured features and mesoporous morphology. Such features impart large surface areas and allow the anchoring of a large number of dye-sensitizers per unit area with favourable consequences on the efficaciousness with which the desired photoactivated electrochemical process occurs. An important issue related to the employment of nanostructured semiconducting cathodes is the determination of the position of the energy levels for the frontier states directly involved in the exchange of photocarriers with the dye-sensitizer in the excited state. Among nanostructured semiconducting cathodes, nickel oxide having nonstoichiometric features is the most important representative of *p*-type photocathodes due to its intrinsic photoelectroactivity. Other examples of nanostructured photocathodes have been also mentioned in the present review, thus indicating new possible directions of research in the materials science of semiconducting electrodes of *p*-type. Also the most important examples of dye-sensitizers for *p*-type nanostructured electrodes have been reviewed. The aspects of electronic conjugation, presence of spacers and substituents with peculiar electronic effects, and state of surface immobilization have been briefly considered in the analysis of the most important structural factors of the dye-sensitizers, which control the process of charge photogeneration and injection in the photocathode. An aspect that has not been considered in depth is the feasibility of the synthesis and purification methods for purposely designed photo-/electrocatalytic systems for *p*-type semiconductors. In terms of short-term goals, the main purpose of the development of increasingly efficient *p*-DSCs is the achievement of efficiencies comparable to those of the *n*-type counterparts in order to produce tandem devices with efficiencies approaching the theoretical limit.

Competing Interests

The authors declare that they have no competing interests.

Authors' Contributions

Part I has been written and compiled by Alessandro Latini, Carmen Cavallo, and Francesco Di Pascasio who contributed equally to the completion of this first part of the review. Part II has been written and compiled by Danilo Dini and Matteo Bonomo who contributed equally to the completion of this second part of the review.

Acknowledgments

The authors wish to thank the Università di Roma "La Sapienza" for financial support through the Project Ateneo

Table 6: Parameters of the *p*-DSC differing for the nature of the nanostructured photocathodes and dye-sensitizers (Figure 9). The redox shuttles here considered are alternatives to the reference couple I_3^-/I^- here considered for comparative purposes.

Cathode	Sensitizer	Redox couple	η/%	V_{OC}/mV	j_{SC}/mA cm^{-2}	FF/%	Ref.
NiO-SP	PMI-6TTPA	$[Fe(acac)_3]^{0/1-}$	2.51	645	−7.65	51.0	[384]
NiO-SP	PMI-6TTPA	$[Co(en)_3]^{3+/2+}$	1.20	724	−4.11	40.0	[384]
NiO-SP	PMI-6TTPA	I_3^-/I^-	0.60	243	−6.26	39.0	[384]
NiO sol-gel	PMI-6TTPA	Thiolate/disulfide	0.51	285	−5.30	34.0	[399]
NiO-SP[1]	PMI-6TTPA	$[Co(en)_3]^{3+/2+}$	1.30	709	−4.44	42.0	[385]
NiO-SP[2]	PMI-6TTPA	$[Co(en)_3]^{3+/2+}$	1.30	660	−4.35	46.0	[385]
$CuCrO_2$[3]	P1	Thiolate/disulfide	0.17	309	−1.43	38.0	[400]
$CuCrO_2$[4]	P1	Thiolate/disulfide	0.17	240	−1.89	36.0	[400]
$CuCrO_2$[5]	P1	Thiolate/disulfide	0.22	293	−1.71	43.0	[400]
$CuCrO_2$[6]	P1	Thiolate/disulfide	0.23	304	−1.73	44.0	[400]
NiO-SP	P1	$[Co(dtbpy)_3]^{3+/2+}$	0.099	280	−1.18	30.0	[401]
NiO-SP	E1	$[Co(dtbpy)_3]^{3+/2+}$	0.130	320	−0.93	44.0	[401]
NiO-SP	E2	$[Co(dtbpy)_3]^{3+/2+}$	0.102	320	−0.78	41.0	[401]
NiO tmpl[7]	T3	I_3^-/I^-	0.180	144	−4.06	30.8	[402]
NiO tmpl	T3H	I_3^-/I^-	0.226	133	−5.56	30.5	[402]
NiO tmpl	T4	I_3^-/I^-	0.207	152	−3.94	34.5	[402]
NiO tmpl	T4H	I_3^-/I^-	0.317	152	−6.73	31.0	[402]
NiO np[8]	PMI-6TTPA	I_3^-/I^-	0.45	226	−5.40	36.0	[403]
NiO np	PMI-6TTPA	$[Co(en)_3]^{3+/2+}$	1.00	640	−3.72	42.0	[403]
$CuCrO_2$	PMI-6TTPA	I_3^-/I^-	0.23	268	−1.98	44.0	[403]
$CuCrO_2$	PMI-6TTPA	$[Co(en)_3]^{3+/2+}$	0.48	734	−1.23	53.0	[403]
NiO db[9]	CW1	I_3^-/I^-	0.114	99	−2.66	35.0	[404]
NiO db	CW2	I_3^-/I^-	0.160	93	−4.05	34.0	[404]
NiO db	P1	I_3^-/I^-	0.143	93	−4.67	33.0	[404]
NiO	BH2	I_3^-/I^-	0.13	97	−4.3	31.0	[405]
NiO	BH4	I_3^-/I^-	0.28	128	−7.4	30.0	[405]
NiO	BH6	I_3^-/I^-	0.13	95	−4.4	31.0	[405]
NiO db	QT1	I_3^-/I^-	0.33	120	−8.2	34.0	[406]
NiO db	QT1	$Co^{3+/2+}$	0.50	226	−6.5	34.0	[406]
$CuCrO_2$	P1	Thiolate/disulfide	0.17	309	−1.43	38.0	[407]
$CuCrO_2$/Au	P1	Thiolate/disulfide	0.31	305	−2.68	38.0	[407]
NiO cl+mp[10]	P1	PCBM	—	620	−0.05	—	[408]
NiO-SP	DPP-1	$[Co(dtbbpy)_3]^{3+/2+}$	0.205	330	−2.06	30.0	[240]
NiO-SP	DPP-2	$[Co(dtbbpy)_3]^{3+/2+}$	0.21	370	−1.95	29.0	[240]
NiO-SP	DPP-NDI	$[Co(dtbbpy)_3]^{3+/2+}$	0.13	292	−1.56	29.0	[240]

SP: screen printed; 1: 0.1 M LiTFSI; 2: 0.5 M LiTFSI; 3: 1.8 μm thick; 4: 3 μm thick; 5: PEDOT counter electrode; 6: CoS counter electrode; 7: tmpl, template [93]; 8: np, nanoparticles; 9: db, doctor blade; 10: cl+mp, mesoporous layer over a compact layer.

Table 7: Parameters of the *t*-DSC differing for the combination of the nanostructured electrodes and corresponding dye-sensitizers. The redox shuttle is represented by the couple I_3^-/I^- if not otherwise indicated. The photoanodic material is mesoporous TiO_2. The *t*-DSC is illuminated from the side of the *n*-electrode (TiO_2 photoanode).

Cathode	*p*-sensitizer	*n*-sensitizer	η/%	V_{OC}/mV	j_{SC}/mA cm^{-2}	FF/%	Ref.
NiO	PMI-6T-TPA	SQ2	1.19	924	1.9	67	[399]
NiO[a]	PMI-6T-TPA	SQ2	1.33	814	2.5	65	[399]
NiO	CAD 3	D35	1.7	613	5.15	54	[265]
NiO	GS 1	D35	1.3	638	4.54	43	[265]
NiO	P1	D35	1.1	732	3.71	38	[265]
NiO	**3**	N719	1.91	1079	2.40	74	[266]
NiO[b]	PMI-NDI	N719	0.55	910	0.97	62	[266]
Se		N719	0.98	940	2.72	39	[409]
NiO	MC[c]	N3[d]	0.66	918	3.62	19	[267]
NiO	ERY B[e]	N719	0.39	732	2.15		[268]

a: cell utilizing thiolate/disulfide redox mediator; b: cell employing $Co^{3+/2+}$ as redox shuttle; c: MC, 3-carboxymethyl-5-[2-(3-octadecyl-2-benzothiazolinyldene) ethylidene]-2-thioxo-4-thiazolidine; d: N3, cis-di(thiocyanato)bis(4,4′-dicarboxy-2-2′-bipyridine) ruthenium(II); e: ERY B, erythrosine b.

Sapienza (Protocol no. 2011/VG1-C26A11PKS2). Moreover, the authors gratefully acknowledge the financial support from Ministero dell'Istruzione dell'Università e della Ricerca-MIUR (Project Title: DSSCX; Protocol no. PRIN 2010-2011, 20104XET32). Danilo Dini wishes to thank Professor J. G. Vos at the School of Chemical Sciences of Dublin City University (DCU), Ireland, for profitable discussion.

References

[1] M. Grätzel, "Conversion of sunlight to electric power by nanocrystalline dye-sensitized solar cells," *Journal of Photochemistry and Photobiology A: Chemistry*, vol. 164, no. 1–3, pp. 3–14, 2004.

[2] B. O'Regan and M. Grätzel, "A low-cost, high-efficiency solar cell based on dye-sensitized colloidal TiO_2 films," *Nature*, vol. 353, no. 6346, pp. 737–740, 1991.

[3] A. Green, K. Emery, Y. Hishikawa, W. Warta, and E. D. Dunlop, "Solar cell efficiency tables (Version 45)," *Progress in Photovoltaics: Research and Application*, vol. 24, pp. 3–11, 2015.

[4] S. Mathew, A. Yella, P. Gao et al., "Dye-sensitized solar cells with 13% efficiency achieved through the molecular engineering of porphyrin sensitizers," *Nature Chemistry*, vol. 6, pp. 242–248, 2014.

[5] http://taf.fi/en/millennium-technology-prize/winners-2010/.

[6] M. Nisha, S. Anusha, A. Antony, R. Manoj, and M. K. Jayaraj, "Effect of substrate temperature on the growth of ITO thin films," *Applied Surface Science*, vol. 252, no. 5, pp. 1430–1435, 2005.

[7] B.-X. Lei, J.-Y. Liao, R. Zhang, J. Wang, C.-Y. Su, and D.-B. Kuang, "Ordered crystalline TiO_2 nanotube arrays on transparent FTO glass for efficient dye-sensitized solar cells," *The Journal of Physical Chemistry C*, vol. 114, no. 35, pp. 15228–15233, 2010.

[8] M. K. Nazeeruddin, A. Kay, I. Rodicio et al., "Conversion of light to electricity by cis-X2bis(2,2'-bipyridyl-4,4'-dicarboxylate)ruthenium(II) charge-transfer sensitizers (X = Cl-, Br-, I-, CN-, and SCN-) on nanocrystalline TiO_2 electrodes," *Journal of the American Chemical Society*, vol. 115, no. 14, pp. 6382–6390, 1993.

[9] M. K. Nazeeruddin, S. M. Zakeeruddin, R. Humphry-Baker et al., "Acid-base equilibria of (2,2′-bipyridyl-4,4′-dicarboxylic acid)ruthenium(II) complexes and the effect of protonation on charge-transfer sensitization of nanocrystalline titania," *Inorganic Chemistry*, vol. 38, no. 26, pp. 6298–6305, 1999.

[10] M. K. Nazeeruddin, P. Pechy, and M. Grätzel, "Efficient panchromatic sensitization of nanocrystalline TiO_2 films by a black dye based on a trithiocyanato-ruthenium complex," *Chemical Communication*, no. 18, pp. 1705–1706, 1997.

[11] P. Wang, C. Klein, R. Humphry-Baker, S. M. Zakeeruddin, and M. Grätzel, "A high molar extinction coefficient sensitizer for stable dye-sensitized solar cells," *Journal of the American Chemical Society*, vol. 127, no. 3, pp. 808–809, 2005.

[12] C.-Y. Chen, M. Wang, J.-Y. Li et al., "Highly efficient light-harvesting ruthenium sensitizer for thin-film dye-sensitized solar cells," *ACS Nano*, vol. 3, no. 10, pp. 3103–3109, 2009.

[13] F. Gao, Y. Wang, D. Shi et al., "Enhance the optical absorptivity of nanocrystalline TiO_2 film with high molar extinction coefficient ruthenium sensitizers for high performance dye-sensitized solar cells," *Journal of the American Chemical Society*, vol. 130, no. 32, pp. 10720–10728, 2008.

[14] J. Wu, Z. Lan, S. Hao et al., "Progress on the electrolytes for dye-sensitized solar cells," *Pure and Applied Chemistry*, vol. 80, no. 11, pp. 2241–2258, 2008.

[15] A. Latini, F. K. Aldibaja, C. Cavallo, and D. Gozzi, "Benzonitrile based electrolytes for best operation of dye sensitized solar cells," *Journal of Power Sources*, vol. 269, pp. 308–316, 2014.

[16] M. Grätzel, "Dye-sensitized solar cells," *Journal of Photochemistry and Photobiology C: Photochemistry Reviews*, vol. 4, no. 2, pp. 145–153, 2003.

[17] M. Ye, X. Wen, M. Wang et al., "Recent advances in dye-sensitized solar cells: from photoanodes, sensitizers and electrolytes to counter electrodes," *Materials Today*, vol. 18, no. 3, pp. 155–162, 2015.

[18] S. C. T. Lau, J. Dayou, C. S. Sipaut, and R. F. Mansa, "Development in photoanode materials for high efficiency dye sensitized solar cells," *International Journal of Renewable Energy Research*, vol. 4, no. 3, pp. 665–674, 2014.

[19] J. Maçaira, L. Andrade, and A. Mendes, "Review on nanostructured photoelectrodes for next generation dye-sensitized solar cells," *Renewable and Sustainable Energy Reviews*, vol. 27, pp. 334–349, 2013.

[20] M. Faraday, *Experimental Researches in Electricity*, vol. 1, Bernard Quaritch, London, UK, 1839.

[21] G. L. Pearson and W. H. Brattain, "History of semiconductor research," *Proceedings of the IRE*, vol. 43, no. 12, pp. 1794–1806, 1955.

[22] D. B. Fahlman, *Materials Chemistry*, Springer, Berlin, Germany, 2007.

[23] A. Hamnett, *Comprehensive Chemical Kinetics*, vol. 27, Elsevier, Amsterdam, The Netherlands, 1987.

[24] J. S. Newman, *Electrochemical System*, Prentice-Hall, Englewood Cliffs, NJ, USA, 1991.

[25] I. Tiginyanu, S. Langa, H. Foell, and V. Ursachi, "Porous III-V Semiconductors," 2009, http://www.porous-35.com/.

[26] X. T. Ming, "Principles and Application of Semicondutor: photoelectrochemistry," *Progress in Inorganic Chemistry*, vol. 41, p. 52, 1994.

[27] K. Rajeshwar, *Fundamentals of Semiconductor Electrochemistry and Photoelectrochemistry*, Encyclopedia of Electrochemistry, 2002.

[28] A. W. Bott, "Electrochemestry of semuconductors," *Current Separation*, vol. 17, no. 3, pp. 87–91, 1998.

[29] M. Chamarro, C. Gourdon, P. Lavallard, O. Lublinskaya, and A. I. Ekimov, "Enhancement of electron-hole exchange interaction in CdSe nanocrystals: a quantum confinement effect," *Physical Review B*, vol. 53, no. 3, pp. 1336–1342, 1996.

[30] Y. Gu, I. L. Kuskovsky, M. Yin, S. O'Brien, and G. F. Neumark, "Quantum confinement in ZnO nanorods," *Applied Physics Letters*, vol. 85, no. 17, pp. 3833–3835, 2004.

[31] B. Delley and E. F. Steigmeier, "Quantum confinement in Si nanocrystals," *Physical Review B*, vol. 47, no. 3, pp. 1397–1400, 1993.

[32] J. Joannopoulos and J. Winn, *Photonic Crystals: Molding the Flow of Light*, Photonic Crystals: Molding the Flow of Light, 2008.

[33] E. Kumacheva, R. K. Golding, M. Allard, and E. H. Sargent, "Colloid crystal growth on mesoscopically patterned surfaces: effect of confinement," *Advanced Materials*, vol. 14, no. 3, pp. 221–224, 2002.

[34] M. Rajalakshmi, A. K. Arora, B. S. Bendre, and S. Mahamuni, "Optical phonon confinement in zinc oxide nanoparticles," *Journal of Applied Physics*, vol. 87, no. 5, pp. 2445–2448, 2000.

[35] A. Yamilov, X. Wu, X. Liu, R. P. H. Chang, and H. Cao, "Self-optimization of optical confinement in an ultraviolet photonic crystal slab laser," *Physical Review Letters*, vol. 96, no. 8, Article ID 083905, 4 pages, 2006.

[36] S. S. Fan, M. G. Chapline, N. R. Franklin, T. W. Tombler, A. M. Cassell, and H. J. Dai, "Self-oriented regular arrays of carbon nanotubes and their field emission properties," *Science*, vol. 283, no. 5401, pp. 512–514, 1999.

[37] Q. F. Zhang, C. S. Dandeneau, X. Y. Zhou, and G. Z. Cao, "ZnO nanostructures for dye-sensitized solar cells," *Advanced Materials*, vol. 21, no. 41, pp. 4087–4108, 2009.

[38] M. Grundmann, *Nano-Optoelectronics: Concepts, Physics and Devices*, Springer, Berlin, Germany, 2002.

[39] F. Patolsky and C. M. Lieber, "Nanowire nanosensors," *Materials Today*, vol. 8, no. 4, pp. 20–28, 2005.

[40] M. Grätzel, "Photoelectrochemical cells," *Nature*, vol. 414, no. 6861, pp. 338–344, 2001.

[41] B. Ohtani, Y. Ogawa, and S.-I. Nishimoto, "Photocatalytic activity of amorphous-anatase mixture of titanium(IV) oxide particles suspended in aqueous solutions," *Journal of Physical Chemistry B*, vol. 101, no. 19, pp. 3746–3752, 1997.

[42] A. Bahramian, "High conversion efficiency of dye-sensitized solar cells based on coral-like TiO_2 nanostructured films: synthesis and physical characterization," *Industrial and Engineering Chemistry Research*, vol. 52, no. 42, pp. 14837–14846, 2013.

[43] H.-P. Wu, C.-M. Lan, J.-Y. Hu et al., "Hybrid titania photoanodes with a nanostructured multi-layer configuration for highly efficient dye-sensitized solar cells," *Journal of Physical Chemistry Letters*, vol. 4, no. 9, pp. 1570–1577, 2013.

[44] Z. Q. Bao, H. Xie, Q. Zhu, J. Qian, P. Ruan, and X. Zhou, "Microsphere assembly of TiO_2 with tube-in-tube nanostructures: anisotropic etching and photovoltaic enhancement," *CrystEngComm*, vol. 15, no. 44, pp. 8972–8978, 2013.

[45] N. Mir, K. Lee, I. Paramasivam, and P. Schmuki, "Optimizing TiO_2 nanotube top geometry for use in dye-sensitized solar cells," *Chemistry—A European Journal*, vol. 18, no. 38, pp. 11862–11866, 2012.

[46] B. H. Lee, M. Y. Song, S.-Y. Jang, S. M. Jo, S.-Y. Kwak, and D. Y. Kim, "Charge transport characteristics of high efficiency dye-sensitized solar cells based on electrospun TiO_2 nanorod photoelectrodes," *The Journal of Physical Chemistry C*, vol. 113, no. 51, pp. 21453–21457, 2009.

[47] E. N. Kumar, R. Jose, P. S. Archana, C. Vijila, M. M. Yusoff, and S. Ramakrishna, "High performance dye-sensitized solar cells with record open circuit voltage using tin oxide nanoflowers developed by electrospinning," *Energy and Environmental Science*, vol. 5, no. 1, pp. 5401–5407, 2012.

[48] J. Huo, Y. Hu, H. Jiang et al., "Mixed solvents assisted flame spray pyrolysis synthesis of TiO_2 hierarchically porous hollow spheres for dye-sensitized solar cells," *Industrial and Engineering Chemistry Research*, vol. 52, no. 32, pp. 11029–11035, 2013.

[49] H.-J. Son, C. Prasittichai, J. E. Mondloch et al., "Dye stabilization and enhanced photoelectrode wettability in water-based dye-sensitized solar cells through post-assembly atomic layer deposition of TiO_2," *Journal of the American Chemical Society*, vol. 135, no. 31, pp. 11529–11532, 2013.

[50] N. Asim, S. Ahmadi, M. A. Alghoul, F. Y. Hammadi, K. Saeedfar, and K. Sopian, "Research and development aspects on chemical preparation techniques of photoanodes for dye sensitized solar cells," *International Journal of Photoenergy*, vol. 2014, Article ID 518156, 21 pages, 2014.

[51] M. Perez-Page, E. Yu, J. Li et al., "Template-based syntheses for shape controlled nanostructures," *Advances in Colloid and Interface Science*, vol. 234, pp. 51–79, 2016.

[52] J. Y. Ying and D. M. Antonelli, "Synthesis of hexagonally packed mesoporous TiO_2 by a modified sol-gel method," *Angewandte Chemie—International Edition*, vol. 34, no. 18, pp. 2014–2017, 1995.

[53] D. Grosso, G. J. A. A. Soler-Illia, F. Babonneau et al., "Highly organized mesoporous titania thin films showing mono-oriented 2D hexagonal channels," *Advanced Materials*, vol. 13, no. 14, pp. 1085–1090, 2001.

[54] H.-S. Yun, K. Miyazawa, H. Zhou, I. Honma, and M. Kuwabara, "Synthesis of mesoporous thin TiO_2 films with hexagonal pore structures using triblock copolymer templates," *Advanced Materials*, vol. 13, no. 18, pp. 1377–1380, 2001.

[55] Y. K. Hwang, K. C. Lee, and X. U. Kwon, "Nanoparticle routes to mesoporous titania thin films," *Chemical Communication*, vol. 21, no. 18, pp. 1738–1739, 2001.

[56] M. A. A. Sadatlu and N. Mozaffari, "Synthesis of mesoporous TiO_2 structures through P123 copolymer as the structural directing agent and assessment of their performance in dye-sensitized solar cells," *Solar Energy*, vol. 133, pp. 24–34, 2016.

[57] D. Sengupta, P. Das, B. Mondal, and K. Mukherjee, "Effects of doping, morphology and film-thickness of photo-anode materials for dye sensitized solar cell application—a review," *Renewable and Sustainable Energy Reviews*, vol. 60, pp. 356–376, 2016.

[58] S. Ito, T. N. Murakami, P. Comte et al., "Fabrication of thin film dye sensitized solar cells with solar to electric power conversion efficiency over 10%," *Thin Solid Films*, vol. 516, no. 14, pp. 4613–4619, 2008.

[59] K. Usha, B. Mondal, D. Sengupta, P. Das, K. Mukherjee, and P. Kumbhakar, "Development of multi-layered nanocrystalline TiO_2 thin films for photovoltaic application," *Optical Materials*, vol. 36, no. 6, pp. 1070–1075, 2014.

[60] P. Tiwana, P. Docampo, M. B. Johnston, H. J. Snaith, and L. M. Herz, "Electron mobility and injection dynamics in mesoporous ZnO, SnO_2, and TiO_2 films used in dye-sensitized solar cells," *ACS Nano*, vol. 5, no. 6, pp. 5158–5166, 2011.

[61] D. Sengupta, P. Das, U. Kasinadhuni, B. Mondal, and K. Mukherjee, "Morphology induced light scattering by zinc oxide polydisperse particles: promising for dye sensitized solar cell application," *Journal of Renewable and Sustainable Energy*, vol. 6, no. 6, Article ID 063114, 17 pages, 2014.

[62] Y. Inamddar, N. Beedri, K. Kodam, A. Shaikh, and H. Pathan, "Aggregation of ZnO nanocrystalline using polyol process for dye (reactive red) sensitized solar cell," *Macromolecular Symposia*, vol. 347, no. 1, pp. 52–57, 2015.

[63] X. Chen, Z. Bai, X. Yan et al., "Design of efficient dye-sensitized solar cells with patterned ZnO-ZnS core-shell nanowire array photoanodes," *Nanoscale*, vol. 6, no. 9, pp. 4691–4697, 2014.

[64] D. Barpuzary, A. Banik, A. N. Panda, and M. Qureshi, "Mimicking the heteroleptic dyes for an efficient 1D-ZnO based dye-sensitized solar cell using the homoleptic ruthenium(II) dipyridophenazine complex as a photosensitizer," *The Journal of Physical Chemistry C*, vol. 119, no. 8, pp. 3892–3902, 2015.

[65] L. Lin, X. Peng, S. Chen, B. Zhang, and Y. Feng, "Preparation of diverse flower-like ZnO nanoaggregates for dye-sensitized solar cells," *RSC Advances*, vol. 5, no. 32, pp. 25215–25221, 2015.

[66] C. Y. Jiang, X. W. Sun, G. Q. Lo, D. L. Kwong, and J. X. Wang, "Improved dye-sensitized solar cells with a ZnO-nanoflower photoanode," *Applied Physics Letters*, vol. 90, no. 26, Article ID 263501, 2007.

[67] Y. Shi, C. Zhu, L. Wang et al., "Ultrarapid sonochemical synthesis of ZnO hierarchical structures: from fundamental research to high efficiencies up to 6.42% for quasi-solid dye-sensitized solar cells," *Chemistry of Materials*, vol. 25, no. 6, pp. 1000–1012, 2013.

[68] A. Kay and M. Grätzel, "Dye-sensitized core-shell nanocrystals: improved efficiency of mesoporous tin oxide electrodes coated with a thin layer of an insulating oxide," *Chemistry of Materials*, vol. 14, no. 7, pp. 2930–2935, 2002.

[69] H. J. Snaith and C. Ducati, "SnO-based dye-sensitized hybrid solar cells exhibiting near unity absorbed photon-to-electron conversion efficiency," *Nano Letters*, vol. 38, pp. 598–603, 2010.

[70] A. Asdim, K. Manseki, T. Sugiura, and T. Yoshida, "Microwave synthesis of size-controllable SnO_2 nanocrystals for dye-sensitized solar cells," *New Journal of Chemistry*, vol. 38, no. 2, pp. 598–603, 2014.

[71] D.-Y. Son, C.-R. Lee, H.-W. Shin et al., "Understanding the role of the dye/oxide interface via SnO_2-based MK-2 dye-sensitized solar cells," *Physical Chemistry Chemical Physics*, vol. 17, no. 23, pp. 15193–15200, 2015.

[72] A. Le Viet, R. Jose, M. V. Reddy, B. V. R. Chowdari, and S. Ramakrishna, "Nb_2O_5 photoelectrodes for dye-sensitized solar cells: choice of the polymorph," *The Journal of Physical Chemistry C*, vol. 114, no. 49, pp. 21795–21800, 2010.

[73] R. Ghosh, M. K. Brennaman, T. Uher et al., "Nanoforest Nb_2O_5 photoanodes for dye-sensitized solar cells by pulsed laser deposition," *ACS Applied Materials and Interfaces*, vol. 3, no. 10, pp. 3929–3935, 2011.

[74] X. Jin, C. Liu, J. Xu, Q. Wang, and D. Chen, "Size-controlled synthesis of mesoporous Nb_2O_5 microspheres for dye sensitized solar cells," *RSC Advances*, vol. 4, no. 67, pp. 35546–35553, 2014.

[75] M. Saito and S. Fujihara, "Large photocurrent generation in dye-sensitized ZnO solar cells," *Energy & Environmental Science*, vol. 1, no. 2, pp. 280–283, 2008.

[76] B. Onwona-Agyeman, S. Kaneko, A. Kumara et al., "Sensitization of nanocrystalline SnO_2 films with indoline dyes," *Japanese Journal of Applied Physics Part 2: Letters*, vol. 44, no. 20–23, pp. L731–L733, 2005.

[77] P. Guo and M. A. Aegerter, "RU(II) sensitized Nb_2O_5 solar cell made by the sol-gel process," *Thin Solid Films*, vol. 351, no. 1-2, pp. 290–294, 1999.

[78] T. Prakash, "Review on nanostructured semiconductors for dye sensitized solar cells," *Electronic Materials Letters*, vol. 8, no. 3, pp. 231–243, 2012.

[79] H. Minoura and T. Yoshida, "Electrodeposition of ZnO/dye hybrid thin films for dye-sensitized solar cells," *Electrochemistry*, vol. 76, no. 2, pp. 109–117, 2008.

[80] B. Tan, E. Toman, Y. Li, and Y. Wu, "Zinc stannate (Zn_2SnO_4) dye-sensitized solar cells," *Journal of the American Chemical Society*, vol. 129, no. 14, pp. 4162–4163, 2007.

[81] A. Turkovic and Z. C. Orel, "Dye sensitized solar cells with CeO_2 and mixed CeO_2/SnO_2 photoanodes," *Solar Energy Materials and Solar Cells*, vol. 45, no. 3, pp. 275–281, 1997.

[82] H. Zheng, Y. Tachibana, and K. Kalantar-Zadeh, "Dye-sensitized solar cells based on WO_3," *Langmuir*, vol. 26, no. 24, pp. 19148–19152, 2010.

[83] S. Burnside, J.-E. Moser, K. Brooks, M. Grätzel, and D. Cahen, "Nanocrystalline mesoporous strontium titanate as photoelectrode material for photosensitized solar devices: increasing photovoltage through flatband potential engineering," *The Journal of Physical Chemistry B*, vol. 103, no. 43, pp. 9328–9332, 1999.

[84] K. Sayama, H. Sugihara, and H. Arakawa, "Photoelectrochemical properties of a porous Nb_2O_5 electrode sensitized by a ruthenium dye," *Chemistry of Materials*, vol. 10, no. 12, pp. 3825–3832, 1998.

[85] A. H. Alami, A. Alketbi, J. Abed, and M. Almheiri, "Assessment of Al–Cu–Fe compound for enhanced solar absorption," *Internation Journal of Energy Research*, vol. 40, no. 4, pp. 514–521, 2015.

[86] H. Zheng, J. Z. Ou, M. S. Strano, R. B. Kaner, A. Mitchell, and K. Kalantar-Zadeh, "Nanostructured tungsten oxide—properties, synthesis, and applications," *Advanced Functional Materials*, vol. 21, no. 12, pp. 2175–2196, 2011.

[87] A. Hagfeldt, G. Boschloo, L. Sun, L. Kloo, and H. Pettersson, "Dye-sensitized solar cells," *Chemical Reviews*, vol. 110, no. 11, pp. 6595–6663, 2010.

[88] F. F. Ngaffo, A. P. Caricato, M. Fernandez, M. Martino, and F. Romano, "Structural properties of single and multilayer ITO and TiO_2 films deposited by reactive pulsed laser ablation deposition technique," *Applied Surface Science*, vol. 253, no. 15, pp. 6508–6511, 2007.

[89] L. H. Hu, S. Y. Weng, J. Xiao et al., "Microstructure design on nanoporous TiO_2 photoelectrodes for dye-sensitized solar cell modules," *The Journal Physical Chemistry*, vol. 111, no. 2, pp. 358–362, 2007.

[90] K. Liu, H. Fu, K. Shi, F. Xiao, L. Jing, and B. Xin, "Preparation of large-pore mesoporous nanocrystalline TiO_2 thin films with tailored pore diameters," *The Journal of Physical Chemistry B*, vol. 109, no. 40, pp. 18719–18722, 2005.

[91] J. T. Jiu, S. J. Isoda, F. M. Wang, and M. J. Adachi, "Dye-sensitized solar cells based on a single-crystalline TiO_2 nanorod film," *The Journal of Physical Chemistry B*, vol. 110, no. 5, pp. 2087–2092, 2006.

[92] M. Adachi, Y. Murata, J. Takao, J. Jiu, M. Sakamoto, and F. Wang, "Highly efficient dye-sensitized solar cells with a titania thin-film electrode composed of a network structure of single-crystal-like TiO_2 nanowires made by the 'oriented attachment' mechanism," *Journal of the American Chemical Society*, vol. 126, no. 45, pp. 14943–14949, 2004.

[93] J. Nelson and R. E. Chandler, "Random walk models of charge transfer and transport in dye sensitized systems," *Coordination Chemistry Reviews*, vol. 248, no. 13-14, pp. 1181–1194, 2004.

[94] S. Quaranta, D. Gozzi, M. Tucci, L. Lazzarini, and A. Latini, "Efficiency improvement and full characterization of dye-sensitized solar cells with MWCNT/anatase Schottky junctions," *Journal of Power Sources*, vol. 204, pp. 249–256, 2012.

[95] S. G. Chen, S. Chappel, Y. Diamant, and A. Zaban, "Preparation of Nb_2O_5 coated TiO_2 nanoporous electrodes and their application in dye-sensitized solar cells," *Chemistry of Materials*, vol. 13, no. 12, pp. 4629–4634, 2001.

[96] E. Palomares, J. N. Clifford, S. A. Haque, T. Lutz, and J. R. Durrant, "Control of charge recombination dynamics in dye sensitized solar cells by the use of conformally deposited metal oxide blocking layers," *Journal of the American Chemical Society*, vol. 125, no. 2, pp. 475–482, 2003.

[97] M. K. Nazeeruddin, F. De Angelis, S. Fantacci et al., "Combined experimental and DFT-TDDFT computational study of

photoelectrochemical cell ruthenium sensitizers," *Journal of the American Chemical Society*, vol. 127, no. 48, pp. 16835–16847, 2005.

[98] Y. Chiba, A. Islam, Y. Watanabe, R. Komiya, N. Koide, and L. Han, "Dye-sensitized solar cells with conversion efficiency of 11.1%," *Japanese Journal of Applied Physics Part 2: Letters*, vol. 45, no. 24–28, pp. L638–L640, 2006.

[99] N.-G. Park and K. Kim, "Transparent solar cells based on dye-sensitized nanocrystalline semiconductors," *Physica Status Solidi (A)*, vol. 205, no. 8, pp. 1895–1904, 2008.

[100] N.-G. Park, J. van de Lagemaat, and A. J. Frank, "Comparison of dye-sensitized rutile- and anatase-based TiO_2 solar cells," *The Journal of Physical Chemistry B*, vol. 104, no. 38, pp. 8989–8994, 2000.

[101] J. A. Rodriguez and M. Fernandez-Garcia, "Metal oxide nanoparticles," in *Nanomaterials: Inorganic and Biorganic Perspective*, 2007.

[102] W. Fan, Q. Zhang, and Y. Wang, "Semiconductor-based nanocomposites for photocatalytic H_2 production and CO_2 conversion," *Physical Chemistry Chemical Physics*, vol. 15, no. 8, pp. 2632–2649, 2013.

[103] X. Zhang, F. Liu, Q.-L. Huang, G. Zhou, and Z.-S. Wang, "Dye-sensitized W-doped TiO_2 solar cells with a tunable conduction band and suppressed charge recombination," *The Journal of Physical Chemistry C*, vol. 115, no. 25, pp. 12665–12671, 2011.

[104] K.-P. Wang and H. Teng, "Zinc-doping in TiO_2 films to enhance electron transport in dye-sensitized solar cells under low-intensity illumination," *Physical Chemistry Chemical Physics*, vol. 11, no. 41, pp. 9489–9496, 2009.

[105] A. Latini, C. Cavallo, F. K. Aldibaja et al., "Efficiency improvement of DSSC photoanode by scandium doping of mesoporous titania beads," *The Journal of Physical Chemistry C*, vol. 117, no. 48, pp. 25276–25289, 2013.

[106] G. Schlichthörl, S. Y. Huang, J. Sprague, and A. J. Frank, "Band edge movement and recombination kinetics in dye-sensitized nanocrystalline TiO_2 solar cells: a study by intensity modulated photovoltage spectroscopy," *The Journal of Physical Chemistry B*, vol. 101, no. 41, pp. 8141–8155, 1997.

[107] C. M. Wang and T. E. Mallouk, "Wide-range tuning of the titanium dioxide flat-band potential by adsorption of fluoride and hydrofluoric acid," *The Journal of Physical Chemistry*, vol. 94, no. 10, pp. 4276–4280, 1990.

[108] J. Bandara and U. W. Pradeep, "Tuning of the flat-band potentials of nanocrystalline TiO_2 and SnO_2 particles with an outer-shell MgO layer," *Thin Solid Films*, vol. 517, no. 2, pp. 952–956, 2008.

[109] J. Qu and C. Lai, "One-dimensional TiO_2 nanostructures as photoanodes for dye-sensitized solar cells," *Journal of Nanomaterials*, vol. 2013, Article ID 762730, 11 pages, 2013.

[110] Q. Zhang and G. Cao, "Hierarchically structured photoelectrodes for dye-sensitized solar cells," *Journal of Materials Chemistry*, vol. 21, no. 19, pp. 6769–6774, 2011.

[111] M. Law, L. E. Greene, J. C. Johnson, R. Saykally, and P. Yang, "Nanowire dye-sensitized solar cells," *Nature Materials*, vol. 4, no. 6, pp. 455–459, 2005.

[112] J. B. Baxter and E. S. Adyl, "Nanowires-based dye-sensitized solar cells," *Applied Physics Letter*, vol. 86, no. 5, Article ID 053114, 2005.

[113] A. B. F. Martinson, J. W. Elam, J. T. Hupp, and M. J. Pellin, "ZnO nanotube based dye-sensitized solar cells," *Nano Letters*, vol. 7, no. 8, pp. 2183–2187, 2007.

[114] L. Schlur, A. Carton, P. Lévêque, D. Guillon, and G. Pourroy, "Optimization of a new ZnO nanorods hydrothermal synthesis method for solid state dye sensitized solar cells applications," *The Journal of Physical Chemistry C*, vol. 117, no. 6, pp. 2993–3001, 2013.

[115] S. Ameen, M. S. Akhtar, M. Song, and H. S. Shin, "Vertically aligned ZnO nanorods on hot filament chemical vapor deposition grown graphene oxide thin film substrate: solar energy conversion," *ACS Applied Materials and Interfaces*, vol. 4, no. 8, pp. 4405–4412, 2012.

[116] M. McCune, W. Zhang, and Y. Deng, "High efficiency dye-sensitized solar cells based on three-dimensional multilayered ZnO nanowire arrays with 'caterpillar-like' structure," *Nano Letters*, vol. 12, no. 7, pp. 3656–3662, 2012.

[117] D. Guo, J. Wang, C. Cui et al., "ZnO@TiO_2 core-shell nanorod arrays with enhanced photoelectrochemical performance," *Solar Energy*, vol. 95, pp. 237–245, 2013.

[118] X. Fang, Y. Li, S. Zhang, L. Bai, N. Yuan, and J. Ding, "The dye adsorption optimization of ZnO nanorod-based dye-sensitized solar cells," *Solar Energy*, vol. 105, pp. 14–19, 2014.

[119] I.-D. Kim, J.-M. Hong, B. H. Lee et al., "Dye-sensitized solar cells using network structure of electrospun ZnO nanofiber mats," *Applied Physics Letters*, vol. 91, no. 16, Article ID 163109, 2007.

[120] W. K. Tan, Z. Lockman, K. Abdul Razak, G. Kawamura, H. Muto, and A. Matsuda, "Enhanced dye-sensitized solar cells performance of ZnO nanorod arrays grown by low-temperature hydrothermal reaction," *International Journal of Energy Research*, vol. 37, no. 15, pp. 1992–2000, 2013.

[121] Z. Yang, T. Xu, Y. Ito, U. Welp, and W. K. Kwok, "Enhanced electron transport in dye-sensitized solar cells using short ZnO nanotips on a rough metal anode," *Journal of Physical Chemistry C*, vol. 113, no. 47, pp. 20521–20526, 2009.

[122] J. Fang, H. Fan, H. Tian, and G. Dong, "Morphology control of ZnO nanostructures for high efficient dye-sensitized solar cells," *Materials Characterization*, vol. 108, pp. 51–57, 2015.

[123] J. Qiu, F. Zhuge, K. Lou et al., "A facile route to aligned TiO_2 nanotube arrays on transparent conducting oxide substrates for dye-sensitized solar cells," *Journal of Materials Chemistry*, vol. 21, no. 13, pp. 5062–5068, 2011.

[124] H.-Y. Chen, T.-L. Zhang, J. Fan, D.-B. Kuang, and C.-Y. Su, "Electrospun hierarchical TiO_2 nanorods with high porosity for efficient dye-sensitized solar cells," *ACS Applied Materials and Interfaces*, vol. 5, no. 18, pp. 9205–9211, 2013.

[125] K. Zhu, N. R. Neale, A. Miedaner, and A. J. Frank, "Enhanced charge-collection efficiencies and light scattering in dye-sensitized solar cells using oriented TiO_2 nanotubes arrays," *Nano Letters*, vol. 7, no. 1, pp. 69–74, 2007.

[126] P. Roy, D. Kim, K. Lee, E. Spiecker, and P. Schmuki, "TiO_2 nanotubes and their application in dye-sensitized solar cells," *Nanoscale*, vol. 2, no. 1, pp. 45–59, 2010.

[127] M. M. Momeni, "Dye-sensitized solar cells based on Cr-doped TiO_2 nanotube photoanodes," *Rare Metals*, 2016.

[128] H. Y. Hwang, A. A. Prabu, D. Y. Kim, and K. J. Kim, "Influence of the organic electrolyte and anodization conditions on the preparation of well-aligned TiO_2 nanotube arrays in dye-sensitized solar cells," *Solar Energy*, vol. 85, no. 7, pp. 1551–1559, 2011.

[129] M. F. Hossain, S. Biswas, Z. H. Zhang, and T. Takahashi, "Bubble-like CdSe nanoclusters sensitized TiO_2 nanotube arrays for improvement in solar cell," *Journal of Photochemistry and Photobiology A: Chemistry*, vol. 217, no. 1, pp. 68–75, 2011.

[130] Y. Hao, Y. Cao, B. Sun, Y. Li, Y. Zhang, and D. Xu, "A novel semiconductor-sensitized solar cell based on P3HT@CdS@TiO_2 core-shell nanotube array," *Solar Energy Materials and Solar Cells*, vol. 101, pp. 107–113, 2012.

[131] J.-Y. Hwang, S.-A. Lee, Y. H. Lee, and S.-I. Seok, "Improved photovoltaic response of nanocrystalline CdS-sensitized solar cells through interface control," *ACS Applied Materials and Interfaces*, vol. 2, no. 5, pp. 1343–1348, 2010.

[132] H. J. Lee, J. Bang, J. Park, S. Kim, and S.-M. Park, "Multilayered semiconductor (CdS/CdSe/ZnS)-sensitized TiO_2 mesoporous solar cells: all prepared by successive ionic layer adsorption and reaction processes," *Chemistry of Materials*, vol. 22, no. 19, pp. 5636–5643, 2010.

[133] M. M. Momeni, "Dye-sensitized solar cells based on tungsten trioxide-titanium dioxide nanotube nanocomposite photoanodes," *Materials Research Innovations*, vol. 20, no. 3, pp. 211–215, 2016.

[134] Y.-L. Xie, Z.-X. Li, Z.-G. Xu, and H.-L. Zhang, "Preparation of coaxial TiO_2/ZnO nanotube arrays for high-efficiency photoenergy conversion applications," *Electrochemistry Communications*, vol. 13, no. 8, pp. 788–791, 2011.

[135] Y. Qiu, W. Chen, and S. Yang, "Double-layered photoanodes from variable-size anatase TiO_2 nanospindles: a candidate for high-efficiency dye-sensitized solar cells," *Angewandte Chemie—International Edition*, vol. 49, no. 21, pp. 3675–3679, 2010.

[136] D. Wu, F. Zhu, J. Li et al., "Monodisperse TiO_2 hierarchical hollow spheres assembled by nanospindles for dye-sensitized solar cells," *Journal of Materials Chemistry*, vol. 22, no. 23, pp. 11665–11671, 2012.

[137] S. Chuangchote, T. Sagawa, and S. Yoshikawa, "Efficient dye-sensitized solar cells using electrospun TiO_2 nanofibers as a light harvesting layer," *Applied Physics Letter*, vol. 93, no. 3, Article ID 033310, 2010.

[138] H.-J. Koo, Y. J. Kim, Y. H. Lee, W. I. Lee, K. Kim, and N.-G. Park, "Nano-embossed hollow spherical TiO_2 as bifunctional material for high-efficiency dye-sensitized solar cells," *Advanced Materials*, vol. 20, no. 1, pp. 195–199, 2008.

[139] C.-Y. Liao, S.-T. Wang, F.-C. Chang, H. P. Wang, and H.-P. Lin, "Preparation of TiO_2 hollow spheres for DSSC photoanodes," *Journal of Physics and Chemistry of Solids*, vol. 75, no. 1, pp. 38–41, 2014.

[140] Y. L. Zhao, D. M. Song, Y. H. Qiang, X. Q. Gu, L. Zhu, and C. B. Song, "Dye-sensitized solar cells based on TiO_2 hollow spheres/TiO_2 nanotube array composite films," *Applied Surface Science*, vol. 309, pp. 85–89, 2014.

[141] L. Xin, Y. Liu, B. Li et al., "Constructing hierarchical submicrotubes from interconnected TiO_2 nanocrystals for high reversible capacity and long-life lithium-ion batteries," *Scientific Reports*, vol. 4, article 4479, 7 pages, 2014.

[142] Y. Wang, H. Huang, P. Zhao et al., "A general precursor strategy for one-dimensional titania with surface nanoprotrusion and tunable structural hierarchy," *CrystEngComm*, vol. 18, no. 8, pp. 1321–1328, 2016.

[143] S. Zhu, L. Shan, X. Tian et al., "Hydrothermal synthesis of oriented ZnO nanorod-nanosheets hierarchical architecture on zinc foil as flexible photoanodes for dye-sensitized solar cells," *Ceramics International*, vol. 40, no. 8, pp. 11663–11670, 2014.

[144] Q. Zhang and G. Cao, "Nanostructured photoelectrodes for dye-sensitized solar cells," *Nano Today*, vol. 6, no. 1, pp. 91–109, 2011.

[145] F. Xu, Y. Wu, X. Zhang, Z. Gao, and K. Jiang, "Controllable synthesis of rutile TiO_2 nanorod array, nanoflowers and microspheres directly on fluorine-doped tin oxide for dye-sensitised solar cells," *Micro & Nano Letters*, vol. 7, no. 8, pp. 826–830, 2012.

[146] C. S. Lee, J. K. Kim, J. Y. Lim, and J. H. Kim, "One-step process for the synthesis and deposition of anatase, two-dimensional, disk-shaped TiO_2 for dye-sensitized solar cells," *ACS Applied Materials and Interfaces*, vol. 6, no. 23, pp. 20842–20850, 2014.

[147] J. Lin, Y. Peng, A. R. Pascoe et al., "A Bi-layer TiO_2 photoanode for highly durable, flexible dye-sensitized solar cells," *Journal of Materials Chemistry A*, vol. 3, no. 8, pp. 4679–4686, 2015.

[148] M. Shanmugam, R. Jacobs-Gedrim, C. Durcan, and B. Yu, "2D layered insulator hexagonal boron nitride enabled surface passivation in dye sensitized solar cells," *Nanoscale*, vol. 5, no. 22, pp. 11275–11282, 2013.

[149] C.-H. Ku and J.-J. Wu, "Chemical bath deposition of ZnO nanowire-nanoparticle composite electrodes for use in dye-sensitized solar cells," *Nanotechnology*, vol. 18, no. 50, pp. 505706–505715, 2007.

[150] Y. Alivov and Z. Y. Fan, "Efficiency of dye sensitized solar cells based on TiO_2 nanotubes filled with nanoparticles," *Applied Physics Letters*, vol. 95, no. 6, pp. 063504–063506, 2009.

[151] K. Mahmood, H. W. Kang, R. Munir, and H. J. Sung, "A dual-functional double-layer film with indium-doped ZnO nanosheets/nanoparticles structured photoanodes for dye-sensitized solar cells," *RSC Advances*, vol. 3, no. 47, pp. 25136–25144, 2013.

[152] U. Mehmood, S. Rahman, K. Harrabi, I. A. Hussein, and B. V. S. Redd, "Recent advances in dye sensitized solar cells," *Advances in Materials Science and Engineering*, vol. 2014, Article ID 974782, 12 pages, 2014.

[153] J.-Y. Liao, J.-W. He, H. Xu, D.-B. Kuang, and C.-Y. Su, "Effect of TiO_2 morphology on photovoltaic performance of dye-sensitized solar cells: nanoparticles, nanofibers, hierarchical spheres and ellipsoid spheres," *Journal of Materials Chemistry*, vol. 22, no. 16, pp. 7910–7918, 2012.

[154] W. Chen and S. Yang, "Dye-sensitized solar cells based on ZnO nanotetrapods," *Frontiers of Optoelectronics in China*, vol. 4, no. 1, pp. 24–44, 2011.

[155] Y. C. Qiu, W. Chen, and S. H. Yang, "Facile hydrothermal preparation of hierarchically assembled, porous single-crystalline ZnO nanoplates and their application in dye-sensitized solar cells," *Journal of Materials Chemistry*, vol. 20, no. 5, pp. 1001–1006, 2010.

[156] W. Chen, H. F. Zhang, I. M. Hsing, and S. H. Yang, "A new photoanode architecture of dye sensitized solar cell based on ZnO nanotetrapods with no need for calcination," *Electrochemistry Communications*, vol. 11, no. 5, pp. 1057–1060, 2009.

[157] W. Chen, Y. C. Qiu, Y. C. Zhong, K. S. Wong, and S. H. Yang, "High-efficiency dye-sensitized solar cells based on the composite photoanodes of SnO_2 nanoparticles/ZnO nanotetrapods," *The Journal of Physical Chemistry A*, vol. 114, no. 9, pp. 3127–3138, 2010.

[158] W. Chen, Y. Qiu, and S. Yang, "A new ZnO nanotetrapods/SnO_2 nanoparticles composite photoanode for high efficiency flexible dye-sensitized solar cells," *Physical Chemistry Chemical Physics*, vol. 12, no. 32, pp. 9494–9501, 2010.

[159] C.-T. Wu, W.-P. Liao, and J.-J. Wu, "Three-dimensional ZnO nanodendrite/nanoparticle composite solar cells," *Journal of Materials Chemistry*, vol. 21, no. 9, pp. 2871–2876, 2011.

[160] F. Sauvage, F. Di Fonzo, A. Li Bassi et al., "Hierarchical TiO_2 photoanode for dye-sensitized solar cells," *Nano Letters*, vol. 10, no. 7, pp. 2562–2567, 2010.

[161] C. A. Grimes, O. K. Varghese, and S. Ranjan, *Light, Water, Hydrogen. The Solar Generation of Hydrogen by Water Photoelectrolysis*, Springer, New York, NY, USA, 2007.

[162] W. Yang, Y. Xu, Y. Tang et al., "Three-dimensional self-branching anatase TiO_2 nanorods: morphology control, growth mechanism and dye-sensitized solar cell application," *Journal of Materials Chemistry A*, vol. 2, no. 38, pp. 16030–16038, 2014.

[163] S. S. Mali, H. Kim, C. S. Shim, P. S. Patil, J. H. Kim, and C. K. Hong, "Surfactant free most probable TiO_2 nanostructures via hydrothermal and its dye sensitized solar cell properties," *Scientific Reports*, vol. 3, article 3004, pp. 1–8, 2013.

[164] Y. L. Zhao, D. S. Yao, C. B. Song et al., "CNT-G-TiO_2layer as a bridge linking TiO_2 nanotube arrays and substrates for efficient dye-sensitized solar cells," *RSC Advances*, vol. 5, no. 54, pp. 43805–43809, 2015.

[165] L.-T. Yan, F.-L. Wu, L. Peng et al., "Photoanode of dye-sensitized solar cells based on a ZnO/TiO_2 composite film," *International Journal of Photoenergy*, vol. 2012, Article ID 613969, 4 pages, 2012.

[166] N. K. Huu, D.-Y. Son, I.-H. Jang, C.-R. Lee, and N.-G. Park, "Hierarchical SnO_2 nanoparticle-ZnO nanorod photoanode for improving transport and life time of photoinjected electrons in dye-sensitized solar cell," *ACS Applied Materials and Interfaces*, vol. 5, no. 3, pp. 1038–1043, 2013.

[167] S. Satapathi, H. S. Gill, S. Das et al., "Performance enhancement of dye-sensitized solar cells by incorporating graphene sheets of various sizes," *Applied Surface Science*, vol. 314, pp. 638–641, 2014.

[168] S. Yang, H. Kou, H. Wang, K. Cheng, and J. Wang, "The photoelectrochemical properties of N_3 sensitized $CaTiO_3$ modified TiO_2 nanocrystalline electrodes," *Electrochimica Acta*, vol. 55, no. 1, pp. 305–310, 2009.

[169] L. Zhang, Y. Shi, S. Peng, J. Liang, Z. Tao, and J. Chen, "Dye-sensitized solar cells made from $BaTiO_3$-coated TiO_2 nanoporous electrodes," *Journal of Photochemistry and Photobiology A: Chemistry*, vol. 197, no. 2-3, pp. 260–265, 2008.

[170] H. A. Moghaddam, M. R. Mohammadi, and S. M. S. Reyhani, "Improved photon to current conversion in nanostructured TiO_2 dye-sensitized solar cells by incorporating cubic $BaTiO_3$ particles deliting incident," *Solar Energy*, vol. 132, pp. 1–14, 2016.

[171] K. Suzuki and K. Kijima, "Optical band gap of barium titanate nanoparticles prepared by RF-plasma chemical vapor deposition," *Japanese Journal of Applied Physics*, vol. 44, no. 4, pp. 2081–2082, 2005.

[172] K. Manoharan and P. Venkatachalam, "Photoelectrochemical performance of dye sensitized solar cells based on aluminum-doped titanium dioxide structures," *Materials Science in Semiconductor Processing*, vol. 30, pp. 208–217, 2015.

[173] K. Song, I. Jang, D. Song, Y. S. Kang, and S.-G. Oh, "Echinoid-like particles with high surface area for dye-sensitized solar cells," *Solar Energy*, vol. 105, pp. 218–224, 2014.

[174] A. H. Ghanbari Niaki, A. M. Bakhshayesh, and M. R. Mohammadi, "Double-layer dye-sensitized solar cells based on Zn-doped TiO_2 transparent and light scattering layers: Improving electron injection and light scattering effect," *Solar Energy*, vol. 103, pp. 210–222, 2014.

[175] S. Y. Choi, M. Mamak, N. Coombs, N. Chopra, and G. A. Ozin, "Thermally stable two-dimensional hexagonal mesoporous nanocrystalline anatase, meso-nc-TiO_2: bulk and crack-free thin film morphologies," *Advanced Functional Materials*, vol. 14, no. 4, pp. 335–344, 2004.

[176] D. G. Shchukin and R. A. Caruso, "Template synthesis and photocatalytic properties of porous metal oxide spheres formed by nanoparticle infiltration," *Chemistry of Materials*, vol. 16, no. 11, pp. 2287–2292, 2004.

[177] M. Iwasaki, S. A. Davis, and S. Mann, "Spongelike macroporous TiO_2 monoliths prepared from starch gel template," *Journal of Sol-Gel Science and Technology*, vol. 32, no. 1–3, pp. 99–105, 2004.

[178] R. A. Caruso and J. H. Schattka, "Cellulose acetate templates for porous inorganic network fabrication," *Advanced Materials*, vol. 12, no. 24, pp. 1921–1923, 2000.

[179] D. Chen, L. Cao, F. Huang, P. Imperia, Y.-B. Cheng, and R. A. Caruso, "Synthesis of monodisperse mesoporous titania beads with controllable diameter, high surface areas, and variable pore diameters (14–23 nm)," *Journal of the American Chemical Society*, vol. 132, no. 12, pp. 4438–4444, 2010.

[180] D. Chen, F. Huang, Y.-B. Cheng, and R. A. Caruso, "Mesoporous anatase TiO_2 beads with high surface areas and controllable pore sizes: a superior candidate for high-performance dye-sensitized solar cells," *Advanced Materials*, vol. 21, no. 21, pp. 2206–2210, 2009.

[181] Y. Saito, S. Kambe, T. Kitamura, Y. Wada, and S. Yanagida, "Morphology control of mesoporous TiO_2 nanocrystalline films for performance of dye-sensitized solar cells," *Solar Energy Materials & Solar Cells*, vol. 83, no. 1, pp. 1–13, 2004.

[182] L. Feng, J. Jia, Y. Fang, X. Zhou, and Y. Lin, "TiO_2 flowers and spheres for ionic liquid electrolytes based dye-sensitized solar cells," *Electrochimica Acta*, vol. 87, pp. 629–636, 2013.

[183] F. Sauvage, D. Chen, P. Comte et al., "Dye-sensitized solar cells employing a single film of mesoporous TiO_2 beads achieve power conversion efficiencies over 10%," *ACS Nano*, vol. 4, no. 8, pp. 4420–4425, 2010.

[184] Y. J. Kim, M. H. Lee, H. J. Kim et al., "Formation of highly efficient dye-sensitized solar cells by hierarchical pore generation with nanoporous TiO_2 spheres," *Advanced Materials*, vol. 21, no. 36, pp. 3618–3673, 2009.

[185] Q. Zhang, T. P. Chou, B. Russo, S. A. Jenekhe, and G. Cao, "Aggregation of ZnO nanocrystallites for high conversion efficiency in dye-sensitized solar cells," *Angewandte Chemie—International Edition*, vol. 47, no. 13, pp. 2402–2406, 2008.

[186] M. Quintana, T. Edvinsson, A. Hagfeldt, and G. Boschloo, "Comparison of dye-sensitized ZnO and TiO_2 solar cells: studies of charge transport and carrier lifetime," *The Journal of Physical Chemistry C*, vol. 111, no. 2, pp. 1035–1041, 2007.

[187] T. P. Chou, Q. F. Zhang, and G. Z. Cao, "Effects of dye loading conditions on the energy conversion efficiency of ZnO and TiO_2 dye-sensitized solar cells," *The Journal of Physical Chemistry C*, vol. 111, no. 50, pp. 18804–18811, 2007.

[188] T. P. Chou, Q. Zhang, G. E. Fryxell, and G. Z. Cao, "Hierarchically structured ZnO film for dye-sensitized solar cells with enhanced energy conversion efficiency," *Advanced Materials*, vol. 19, no. 18, pp. 2588–2592, 2007.

[189] E. J. W. Crossland, N. Noel, V. Sivaram, T. Leijtens, J. A. Alexander-Webber, and H. J. Snaith, "Mesoporous TiO_2 single crystals delivering enhanced mobility and optoelectronic device performance," *Nature*, vol. 495, no. 7440, pp. 215–219, 2013.

[190] A. Latini, R. Panetta, C. Cavallo, D. Gozzi, and S. Quaranta, "A comparison of the performances of different mesoporous titanias in dye-sensitized solar cells," *Journal of Nanomaterials*, vol. 2015, Article ID 450405, 8 pages, 2015.

[191] R. Zhang, B. Tu, and D. Zhao, "Synthesis of highly stable and crystalline mesoporous anatase by using a simple surfactant sulfuric acid carbonization method," *Chemistry—A European Journal*, vol. 16, no. 33, pp. 9977–9981, 2010.

[192] S. Yamazoe, Y. Masutani, T. Shishido, and T. Tanaka, "Metal oxide promoted TiO_2 catalysts for photo-assisted selective catalytic reduction of NO with NH_3," *Research on Chemical Intermediates*, vol. 34, no. 5–7, pp. 487–494, 2008.

[193] H. Wang and J. P. Lewis, "Second-generation photocatalytic materials: anion-doped TiO_2," *Journal of Physics: Condensed Matter*, vol. 18, no. 2, pp. 421–434, 2006.

[194] M. Inagaki, Y. Nakazawa, M. Hirano, Y. Kobayashi, and M. Toyoda, "Preparation of stable anatase-type TiO_2 and its photocatalytic performance," *International Journal of Inorganic Materials*, vol. 3, no. 7, pp. 809–811, 2001.

[195] H. Park, H. S. Jie, B. Neppolian et al., "Preparation of highly active TiO_2 nano-particle photocatalysts by a flame aerosol method for the complete oxidation of 2-propanol," *Topics in Catalysis*, vol. 47, no. 3-4, pp. 166–174, 2008.

[196] M. Hirano, K. Ota, and H. Iwata, "Direct formation of anatase (TiO_2)/silica (SiO_2) composite nanoparticles with high phase stability of 1300°C from acidic solution by hydrolysis under hydrothermal condition," *Chemistry of Materials*, vol. 16, no. 19, pp. 3725–3732, 2004.

[197] M. Hirano and T. Ito, "Direct formation of new, phase-stable, and photoactive anatase-type $Ti_{1-2X}Nb_XSc_XO_2$ solid solution nanoparticles by hydrothermal method," *Materials Research Bulletin*, vol. 43, pp. 2196–2206, 2008.

[198] A. K. Chandiran, F. Sauvage, L. Etgar, and M. Grätzel, "Ga^{3+} and Y^{3+} cationic substitution in mesoporous TiO_2 photoanodes for photovoltaic applications," *The Journal of Physical Chemistry C*, vol. 115, no. 18, pp. 9232–9240, 2011.

[199] A. K. Chandiran, F. Sauvage, M. Casas-Cabanas, P. Comte, S. M. Zakeeruddin, and M. Graetzel, "Doping a TiO_2 photoanode with Nb^{5+} to enhance transparency and charge collection efficiency in dye-sensitized solar cells," *The Journal of Physical Chemistry C*, vol. 114, no. 37, pp. 15849–15856, 2010.

[200] R. Li, Y. Zhao, R. Hou et al., "Enhancement of power conversion efficiency of dye sensitized solar cells by modifying mesoporous TiO_2 photoanode with Al-doped TiO_2 layer," *Journal of Photochemistry and Photobiology A: Chemistry*, vol. 319-320, pp. 62–69, 2016.

[201] M. Hirano and T. Ito, "Effect of co-dopant on the formation and properties of anatase-type titania solid solutions doped with niobium," *Journal of Physics and Chemistry of Solids*, vol. 72, no. 6, pp. 661–666, 2011.

[202] R. T. Ako, P. Ekanayake, A. L. Tan, and D. J. Young, "La modified TiO_2 photoanode and its effect on DSSC performance: a comparative study of doping and surface treatment on deep and surface charge trapping," *Materials Chemistry and Physics*, vol. 172, pp. 105–112, 2016.

[203] G. Liu, L. Wang, H. G. Yang, H.-M. Cheng, and G. Q. Max Lu, "Titania-based photocatalysts—crystal growth, doping and heterostructuring," *Journal of Materials Chemistry*, vol. 20, no. 5, pp. 831–843, 2010.

[204] W. Zhou and H. Fu, "Mesoporous TiO_2: preparation, doping, and as a composite for photocatalysis," *ChemCatChem*, vol. 5, no. 4, pp. 885–894, 2013.

[205] W. Guo, L. Wu, Z. Chen, G. Boschloo, A. Hagfeldt, and T. Ma, "Highly efficient dye-sensitized solar cells based on nitrogen-doped titania with excellent stability," *Journal of Photochemistry and Photobiology A: Chemistry*, vol. 219, no. 2-3, pp. 180–187, 2011.

[206] A. Subramanian and H.-W. Wang, "Effects of boron doping in TiO_2 nanotubes and the performance of dye-sensitized solar cells," *Applied Surface Science*, vol. 258, no. 17, pp. 6479–6484, 2012.

[207] N. T. Hieu, S. J. Baik, O. H. Chung, and J. S. Park, "Fabrication and characterization of electrospun carbon nanotubes/titanium dioxide nanofibers used in anodes of dye-sensitized solar cells," *Synthetic Metals*, vol. 193, pp. 125–131, 2014.

[208] Q. Sun, J. Zhang, P. Wang et al., "Sulfur-doped TiO_2 nanocrystalline photoanodes for dye-sensitized solar cells," *Journal of Renewable and Sustainable Energy*, vol. 4, no. 2, Article ID 023104, 2012.

[209] S. I. Noh, K.-N. Bae, H.-J. Ahn, and T.-Y. Seong, "Improved efficiency of dye-sensitized solar cells through fluorine-doped TiO_2 blocking layer," *Ceramics International*, vol. 39, no. 7, pp. 8097–8101, 2013.

[210] M. Pan, H. Liu, Z. Yao, and X. Zhong, "Enhanced efficiency of dye-sensitized solar cells by trace amount Ca-doping in TiO_2 photoelectrodes," *Journal of Nanomaterials*, vol. 2015, Article ID 974161, 5 pages, 2015.

[211] H. Tian, L. Hu, C. Zhang et al., "Enhanced photovoltaic performance of dye-sensitized solar cells using a highly crystallized mesoporous TiO_2 electrode modified by boron doping," *Journal of Materials Chemistry*, vol. 21, no. 3, pp. 863–868, 2011.

[212] J. Zhang, W. Peng, Z. Chen, H. Chen, and L. Han, "Effect of cerium doping in the TiO_2 photoanode on the electron transport of dye-sensitized solar cells," *The Journal of Physical Chemistry C*, vol. 116, no. 36, pp. 19182–19190, 2012.

[213] C. Kim, K.-S. Kim, H. Y. Kim, and Y. S. Han, "Modification of a TiO_2 photoanode by using Cr-doped TiO_2 with an influence on the photovoltaic efficiency of a dye-sensitized solar cell," *Journal of Materials Chemistry*, vol. 18, no. 47, pp. 5809–5814, 2008.

[214] K. Kakiage, T. Tokutome, S. Iwamoto, T. Kyomen, and M. Hanaya, "Fabrication of a dye-sensitized solar cell containing a Mg-doped TiO_2 electrode and a Br_{3^-}/ Br− redox mediator with a high open-circuit photovoltage of 1.21V," *Chemical Communications*, vol. 49, no. 2, pp. 179–180, 2013.

[215] Y. Xie, N. Huang, Y. Liu et al., "Photoelectrodes modification by N doping for dye-sensitized solar cells," *Electrochimica Acta*, vol. 93, pp. 202–206, 2013.

[216] T. Nikolay, L. Larina, O. Shevaleevskiy, and B. T. Ahn, "Electronic structure study of lightly Nb-doped TiO_2 electrode for dye-sensitized solar cells," *Energy and Environmental Science*, vol. 4, no. 4, pp. 1480–1486, 2011.

[217] S. G. Kim, M. J. Ju, I. T. Choi et al., "Nb-doped TiO_2 nanoparticles for organic dye-sensitized solar cells," *RSC Advances*, vol. 3, no. 37, pp. 16380–16386, 2013.

[218] X. Lü, X. Mou, J. Wu et al., "Improved-performance dye-sensitized solar cells using Nb-doped TiO_2 electrodes: efficient electron injection and transfer," *Advanced Functional Materials*, vol. 20, no. 3, pp. 509–515, 2010.

[219] M. Wang, S. L. Bai, A. F. Chen et al., "Improved photovoltaic performance of dye-sensitized solar cells by Sb-doped TiO_2 photoanode," *Electrochimica Acta*, vol. 77, pp. 54–59, 2012.

[220] Y. Duan, N. Fu, Q. Liu et al., "Sn-doped TiO_2 photoanode for dye-sensitized solar cells," *Journal of Physical Chemistry C*, vol. 116, no. 16, pp. 8888–8893, 2012.

[221] G. Xie, Y. Wei, L. Fan, and J. Wu, "Application of doped rare-earth oxide TiO_2:(Tm^{3+}, Yb^{3+}) in dye-sensitized solar cells," *The Journal of Physics: Conference Series*, vol. 339, Article ID 012010, 2012.

[222] P. Xiang, W. Ma, T. Xiao, L. Jiang, X. Tan, and T. Shu, "Ta-doped hierarchical TiO_2 spheres for dye-sensitized solar cells," *Journal of Alloys and Compounds*, vol. 656, pp. 45–50, 2016.

[223] Z. Tong, T. Peng, W. Sun, W. Liu, S. Guo, and X.-Z. Zhao, "Introducing an intermediate band into dye-sensitized solar cells by W^{6+} doping into TiO_2 nanocrystalline photoanodes," *The Journal of Physical Chemistry C*, vol. 118, no. 30, pp. 16892–16895, 2014.

[224] C. Cavallo, A. Salleo, D. Gozzi et al., "Solid solutions of rare earth cations in mesoporous anatase beads and their performances in dye-sensitized solar cells," *Scientific Reports*, vol. 5, Article ID 16785, 15 pages, 2015.

[225] S. Zhu, X. Tian, L. Shan et al., "Effect of Al^{3+} on the growth of ZnO nanograss film and its application in dye-sensitized solar cells," *Ceramics International*, vol. 39, no. 8, pp. 9637–9644, 2013.

[226] R. Tao, T. Tomita, R. A. Wong, and K. Waki, "Electrochemical and structural analysis of Al-doped ZnO nanorod arrays in dye-sensitized solar cells," *Journal of Power Sources*, vol. 214, pp. 159–165, 2012.

[227] J.-H. Kim, K.-J. Lee, J.-H. Roh et al., "Ga-doped zno transparent electrodes with TiO_2 blocking layer/nanoparticles for dye-sensitized solar cells," *Nanoscale Research Letters*, vol. 7, article 11, no. 1, 2012.

[228] Y.-Z. Zheng, X. Tao, Q. Hou, D.-T. Wang, W.-L. Zhou, and J.-F. Chen, "Iodine-doped ZnO nanocrystalline aggregates for improved dye-sensitized solar cells," *Chemistry of Materials*, vol. 23, no. 1, pp. 3–5, 2011.

[229] J. Bai, X. Xu, L. Xu et al., "Potassium-doped zinc oxide as photocathode material in dye-sensitized solar cells," *ChemSusChem*, vol. 6, no. 4, pp. 622–629, 2013.

[230] C. J. Raj, K. Prabakar, S. N. Karthick, K. V. Hemalatha, M.-K. Son, and H.-J. Kim, "Banyan root structured Mg-Doped Zno photoanode dye-sensitized solar cells," *Journal of Physical Chemistry C*, vol. 117, no. 6, pp. 2600–2607, 2013.

[231] X. Guo, H. Dong, G. Niu, Y. Qiu, and L. Wang, "Mg doping in nanosheet-based spherical structured ZnO photoanode for quasi-solid dye-sensitized solar cells," *RSC Advances*, vol. 4, no. 41, pp. 21294–21300, 2014.

[232] K. Mahmood, B. S. Swain, G.-S. Han, B.-J. Kim, and H. S. Jung, "Polyethylenimine-assisted growth of high-aspect-ratio nitrogen-doped ZnO (NZO) nanorod arrays and their effect on performance of dye-sensitized solar cells," *ACS Applied Materials & Interfaces*, vol. 6, no. 13, pp. 10028–10043, 2014.

[233] M. Bonomo, G. Naponiello, A. Di Carlo, and D. Dini, "Characterization of screen-printed nickel oxide electrodes for p-type dye-sensitized solar cells," *Journal of Material Science and Nanotecnology*, vol. 4, no. 2, pp. 201–218, 2016.

[234] S. Sheehan, G. Naponiello, F. Odobel, D. P. Dowling, A. Di Carlo, and D. Dini, "Comparison of the photoelectrochemical properties of RDS NiO thin films for p-type DSCs with different organic and organometallic dye-sensitizers and evidence of a direct correlation between cell efficiency and charge recombination," *Journal of Solid State Electrochemistry*, vol. 19, no. 4, pp. 975–986, 2015.

[235] M. Awais, D. D. Dowling, F. Decker, and D. Dini, "Photoelectrochemical properties of mesoporous NiO_x deposited on technical FTO via nanopowder sintering in conventional and plasma atmospheres," *SpringerPlus*, vol. 4, no. 1, article 564, 2015.

[236] M. Awais, E. Gibson, J. G. Vos, D. P. Dowling, A. Hagfeldt, and D. Dini, "Fabrication of efficient NiO photocathodes prepared via RDS with novel routes of substrate processing for p-type dye-sensitized solar cells," *ChemElectroChem*, vol. 1, no. 2, pp. 384–391, 2014.

[237] D. Dini, Y. Halpin, J. G. Vos, and E. A. Gibson, "The influence of the preparation method of NiO_x photocathodes on the efficiency of p-type dye-sensitized solar cells," *Coordination Chemistry Reviews*, vol. 304-305, pp. 179–201, 2015.

[238] N. Li, E. A. Gibson, P. Qin et al., "Double-layered NiO photocathodes for p-Type DSSCs with record IPCE," *Advanced Materials*, vol. 22, no. 15, pp. 1759–1762, 2010.

[239] G. H. Summers, J.-F. Lefebvre, F. A. Black et al., "Design and characterisation of bodipy sensitizers for dye-sensitized NiO solar cells," *Physical Chemistry Chemical Physics*, vol. 18, no. 2, pp. 1059–1070, 2015.

[240] M. Gennari, F. Légalité, L. Zhang et al., "Long-lived charge separated state in NiO-based p-type dye-sensitized solar cells with simple cyclometalated iridium complexes," *Journal of Physical Chemistry Letters*, vol. 5, no. 13, pp. 2254–2258, 2014.

[241] D. Dini, "Nanostructured metal oxide thin films as photoactive cathodes of *P*–type dye– sensitised solar cells," *Physical Chemistry Communication*, vol. 3, no. 1, pp. 14–51, 2016.

[242] T. Daeneke, Z. Yu, G. P. Lee et al., "Dominating energy losses in NiO p-type dye-sensitized solar cells," *Advanced Energy Materials*, vol. 5, no. 4, Article ID 1401387, 2015.

[243] Z. Ji, G. Natu, Z. Huang, and Y. Wu, "Linker effect in organic donor-acceptor dyes for p-type NiO dye sensitized solar cells," *Energy and Environmental Science*, vol. 4, no. 8, pp. 2818–2821, 2011.

[244] M. Congiu, M. Bonomo, M. L. De Marco et al., "Cobalt sulfide as counter electrode in p-type dye-sensitized solar cells," *ChemistrySelect*, vol. 1, no. 11, pp. 2808–2815, 2016.

[245] Z. Ji, G. Natu, Z. Huang, O. Kokhan, X. Zhang, and Y. Wu, "Synthesis, photophysics, and photovoltaic studies of ruthenium cyclometalated complexes as sensitizers for p-type NiO dye-sensitized solar cells," *Journal of Physical Chemistry C*, vol. 116, no. 32, pp. 16854–16863, 2012.

[246] Y. Pellegrin, L. Le Pleux, E. Blart et al., "Ruthenium polypyridine complexes as sensitizers in NiO based p-type dye-sensitized solar cells: effects of the anchoring groups," *Journal of Photochemistry and Photobiology A: Chemistry*, vol. 219, no. 2-3, pp. 235–242, 2011.

[247] M. Awais, D. P. Dowling, F. Decker, and D. Dini, "Electrochemical characterization of nanoporous nickel oxide thin films spray-deposited onto indium-doped tin oxide for solar conversion scopes," *Advances in Condensed Matter Physics*, vol. 2015, Article ID 186375, 18 pages, 2015.

[248] G. Naponiello, I. Venditti, V. Zardetto et al., "Photoelectrochemical characterization of squaraine-sensitized nickel oxide cathodes deposited via screen-printing for p-type dye-sensitized solar cells," *Applied Surface Science*, vol. 356, pp. 911–920, 2015.

[249] M. Awais, D. D. Dowling, M. Rahman, J. G. Vos, F. Decker, and D. Dini, "Spray-deposited NiO_x films on ITO substrates as photoactive electrodes for p-type dye-sensitized solar cells," *Journal of Applied Electrochemistry*, vol. 43, no. 2, pp. 191–197, 2013.

[250] D. Ameline, S. Diring, Y. Farre et al., "Isoindigo derivatives for application in p-type dye sensitized solar cells," *RSC Advances*, vol. 5, no. 104, pp. 85530–85539, 2015.

[251] A. Nattestad, M. Ferguson, R. Kerr, Y.-B. Cheng, and U. Bach, "Dye-sensitized nickel(II)oxide photocathodes for tandem solar cell applications," *Nanotechnology*, vol. 19, no. 29, Article ID 295304, 2008.

[252] L. Zhu, H. B. Yang, C. Zhong, and C. M. Li, "Rational design of triphenylamine dyes for highly efficient p-type dye sensitized solar cells," *Dyes and Pigments*, vol. 105, pp. 97–104, 2014.

[253] J. Warnan, Y. Pellegrin, E. Blart et al., "Acetylacetone anchoring group for NiO-based dye-sensitized solar cell," *Dyes and Pigments*, vol. 105, pp. 174–179, 2014.

[254] Z. Ji, G. Natu, and Y. Wu, "Cyclometalated ruthenium sensitizers bearing a triphenylamino group for p-type NiO dye-sensitized solar cells," *ACS Applied Materials and Interfaces*, vol. 5, no. 17, pp. 8641–8648, 2013.

[255] Z. Liu, D. Xiong, X. Xu et al., "Modulated charge injection in p-type dye-sensitized solar cells using fluorene-based light absorbers," *ACS Applied Materials and Interfaces*, vol. 6, no. 5, pp. 3448–3454, 2014.

[256] J. C. Freys, J. M. Gardner, L. D'Amario, A. M. Brown, and L. Hammarström, "Ru-based donor-acceptor photosensitizer that retards charge recombination in a p-type dye-sensitized solar cell," *Dalton Transactions*, vol. 41, no. 42, pp. 13105–13111, 2012.

[257] L. Favereau, J. Warnan, Y. Pellegrin et al., "Diketopyrrolopyrrole derivatives for efficient NiO-based dye-sensitized solar cells," *Chemical Communications*, vol. 49, no. 73, pp. 8018–8020, 2013.

[258] J. Y. Park, B. Y. Jang, C. H. Lee, H. J. Yun, and J. H. Kim, "Influence of the anchoring number in a carbazole-based photosensitizer on the photovoltaic performance of p-type NiO dye sensitized solar cells," *RSC Advances*, vol. 4, pp. 61248–61255, 2014.

[259] F. Wu, S. Zhao, C. Zhong, Q. Song, and L. Zhu, "Insights into dye design for efficient p-type photoelectrodes: effect of oligothiophene length between the donor and the NiO surface," *RSC Advances*, vol. 5, no. 113, pp. 93652–93658, 2015.

[260] Z. Ji and Y. Wu, "Photoinduced electron transfer dynamics of cyclometalated ruthenium (II)-naphthalenediimide dyad at NiO photocathode," *The Journal of Physical Chemistry C*, vol. 117, no. 36, pp. 18315–18324, 2013.

[261] M. Bonomo, N. Barbero, F. Matteocci, A. D. Carlo, C. Barolo, and D. Dini, "Beneficial effect of electron-withdrawing groups on the sensitizing action of squaraines for p-type dye-sensitized solar cells," *The Journal of Physical Chemistry C*, vol. 120, no. 30, pp. 16340–16353, 2016.

[262] M. He, Z. Ji, Z. Huang, and Y. Wu, "Molecular orbital engineering of a panchromatic cyclometalated Ru(II) dye for p-type dye-sensitized solar cells," *Journal of Physical Chemistry C*, vol. 118, no. 30, pp. 16518–16525, 2014.

[263] F. Wu, J. Liu, X. Li et al., "D–A–A-type organic dyes for NiO-based dye-sensitized solar cells," *European Journal of Organic Chemistry*, vol. 2015, no. 31, pp. 6850–6857, 2015.

[264] H. Tian, J. Oscarsson, E. Gabrielsson et al., "Enhancement of p-type dye-sensitized solar cell performance by supramolecular assembly of electron donor and acceptor," *Scientific Reports*, vol. 4, article 4282, 2014.

[265] C. J. Wood, G. H. Summers, and E. A. Gibson, "Increased photocurrent in a tandem dye-sensitized solar cell by modifications in push–pull dye-design," *Chemical Communications*, vol. 51, no. 18, pp. 3915–3918, 2015.

[266] A. Nattestad, A. J. Mozer, M. K. R. Fischer et al., "Highly efficient photocathodes for dye-sensitized tandem solar cells," *Nature Materials*, vol. 9, no. 1, pp. 31–35, 2010.

[267] A. Nakasa, H. Usami, S. Sumikura, S. Hasegawa, T. Koyama, and E. Suzuki, "A high voltage dye-sensitized solar cell using a nanoporous NiO photocathode," *Chemistry Letters*, vol. 34, no. 4, pp. 500–501, 2005.

[268] J. He, H. Lindström, A. Hagfeldt, and S.-E. Lindquist, "Dye-sensitized nanostructured tandem cell-first demonstrated cell with a dye-sensitized photocathode," *Solar Energy Materials and Solar Cells*, vol. 62, no. 3, pp. 265–273, 2000.

[269] E. A. Gibson, A. L. Smeigh, L. Le Pieux et al., "A p-type NiO-based dye-sensitized solar cell with an open-circuit voltage of 0.35 v," *Angewandte Chemie—International Edition*, vol. 48, no. 24, pp. 4402–4405, 2009.

[270] S. Fiechter, P. Bogdanoff, T. Bak, and J. Nowotny, "Basic concepts of photoelectrochemical solar energy conversion systems," *Advances in Applied Ceramics*, vol. 111, no. 1-2, pp. 39–43, 2012.

[271] Z. Shi, X. Wen, Z. Guan, D. Cao, W. Luo, and Z. Zou, "Recent progress in photoelectrochemical water splitting for solar hydrogen production," *Annals of Physics*, vol. 358, pp. 236–247, 2015.

[272] J. Nowotny, A. J. Atanacio, T. Bak et al., "Photosensitive oxide semiconductors for solar hydrogen fuel and water disinfection," *International Materials Reviews*, vol. 59, no. 8, pp. 449–478, 2014.

[273] C. A. Downes and S. C. Marinescu, "Efficient electrochemical and photoelectrochemical H_2 production from water by a cobalt dithiolene one-dimensional metal-organic surface," *Journal of the American Chemical Society*, vol. 137, no. 43, pp. 13740–13743, 2015.

[274] N. Queyriaux, N. Kaeffer, A. Morozan, M. Chavarot-Kerlidou, and V. Artero, "Molecular cathode and photocathode materials for hydrogen evolution in photoelectrochemical devices," *Journal of Photochemistry and Photobiology C: Photochemistry Reviews*, vol. 205, pp. 90–105, 2015.

[275] Y. Zhao, J. R. Swierk, J. D. Megiatto Jr. et al., "Improving the efficiency of water splitting in dye-sensitized solar cells by using a biomimetic electron transfer mediator," *Proceedings of the National Academy of Sciences of the United States of America*, vol. 109, no. 39, pp. 15612–15616, 2012.

[276] J. Jiao, J. Xia, W. Qiu et al., "Hierarchical tree-like heterostructure arrays for enhanced photoeletrochemical activity," *Electrochimica Acta*, vol. 136, pp. 217–222, 2014.

[277] O. Zandi and T. W. Hamann, "The potential versus current state of water splitting with hematite," *Physical Chemistry Chemical Physics*, vol. 17, no. 35, pp. 22485–22503, 2015.

[278] Y. K. Gaudy and S. Haussener, "Utilizing modeling, experiments, and statistics for the analysis of water-splitting photoelectrodes," *Journal of Materials Chemistry A*, vol. 4, no. 8, pp. 3100–3114, 2016.

[279] M. A. Modestino and S. Haussener, "An integrated device view on photo-electrochemical solar-hydrogen generation," *Annual Review of Chemical and Biomolecular Engineering*, vol. 6, pp. 13–34, 2015.

[280] K. A. Click, D. R. Beauchamp, Z. Huang, W. Chen, and Y. Wu, "Membrane-inspired acidically stable dye-sensitized photocathode for solar fuel production," *Journal of the American Chemical Society*, vol. 138, no. 4, pp. 1174–1179, 2016.

[281] C. G. Morales-Guio, M. T. Mayer, A. Yella, S. D. Tilley, M. Grätzel, and X. Hu, "An optically transparent iron nickel oxide catalyst for solar water splitting," *Journal of the American Chemical Society*, vol. 137, no. 31, pp. 9927–9936, 2015.

[282] B. Kumar, M. Llorente, J. Froehlich, T. Dang, A. Sathrum, and C. P. Kubiak, "Photochemical and photoelectrochemical reduction

of CO_2," *Annual Review of Physical Chemistry*, vol. 63, pp. 541–569, 2012.

[283] H. Tian, "Molecular catalyst immobilized photocathodes for water/proton and carbon dioxide reduction," *ChemSusChem*, vol. 8, no. 22, pp. 3746–3759, 2015.

[284] M. Aresta, A. Dibenedetto, and A. Angelini, "Catalysis for the valorization of exhaust carbon: from CO_2 to chemicals, materials, and fuels. technological use of CO_2," *Chemical Reviews*, vol. 114, no. 3, pp. 1709–1742, 2014.

[285] N. Sutin, C. Creutz, and E. Fujita, "Photo-induced generation of dihydrogen and reduction of carbon dioxide using transition metal complexes," *Comments on Inorganic Chemistry*, vol. 19, no. 2, pp. 67–92, 1997.

[286] K. Tanaka and D. Ooyama, "Multi-electron reduction of CO_2 via Ru-CO_2, -C(O)OH, -CO, -CHO, and -CH_2OH species," *Coordination Chemistry Reviews*, vol. 226, no. 1-2, pp. 211–218, 2002.

[287] W. Leitner, "The coordination chemistry of carbon dioxide and its relevance for catalysis: a critical survey," *Coordination Chemistry Reviews*, vol. 153, pp. 257–284, 1996.

[288] E. E. Benson, C. P. Kubiak, A. J. Sathrum, and J. M. Smieja, "Electrocatalytic and homogeneous approaches to conversion of CO_2 to liquid fuels," *Chemical Society Reviews*, vol. 38, no. 1, pp. 89–99, 2009.

[289] R. P. S. Chaplin and A. A. Wragg, "Effects of process conditions and electrode material on reaction pathways for carbon dioxide electroreduction with particular reference to formate formation," *Journal of Applied Electrochemistry*, vol. 33, no. 12, pp. 1107–1123, 2003.

[290] M. Gattrell, N. Gupta, and A. Co, "A review of the aqueous electrochemical reduction of CO_2 to hydrocarbons at copper," *Journal of Electroanalytical Chemistry*, vol. 594, no. 1, pp. 1–19, 2006.

[291] T. Hatsukade, K. P. Kuhl, E. R. Cave, D. N. Abram, and T. F. Jaramillo, "Insights into the electrocatalytic reduction of CO_2 on metallic silver surfaces," *Physical Chemistry Chemical Physics*, vol. 16, no. 27, pp. 13814–13819, 2014.

[292] A. Begum and P. G. Pickup, "Electrocatalysis of CO_2 reduction by ruthenium benzothiazole and bithiazole complexes," *Electrochemistry Communications*, vol. 9, no. 10, pp. 2525–2528, 2007.

[293] R. Angamuthu, P. Byers, M. Lutz, A. L. Spek, and E. Bouwman, "Electrocatalytic CO_2 conversion to oxalate by a copper complex," *Science*, vol. 327, no. 5963, pp. 313–315, 2010.

[294] V. P. Indrakanti, J. D. Kubicki, and H. H. Schobert, "Photoinduced activation of CO_2 on Ti-based heterogeneous catalysts: current state, chemical physics-based insights and outlook," *Energy and Environmental Science*, vol. 2, no. 7, pp. 745–758, 2009.

[295] M. Mikkelsen, M. Jørgensen, and F. C. Krebs, "The teraton challenge. A review of fixation and transformation of carbon dioxide," *Energy and Environmental Science*, vol. 3, no. 1, pp. 43–81, 2010.

[296] M. Halmann, "Photoelectrochemical reduction of aqueous carbon dioxide on p-type gallium phosphide in liquid junction solar cells," *Nature*, vol. 275, no. 5676, pp. 115–116, 1978.

[297] T. Inoue, A. Fujishima, S. Konishi, and K. Honda, "Photoelectrocatalytic reduction of carbon dioxide in aqueous suspensions of semiconductor powders," *Nature*, vol. 277, no. 5698, pp. 637–638, 1979.

[298] E. E. Barton, D. M. Rampulla, and A. B. Bocarsly, "Selective solar-driven reduction of CO_2 to methanol using a catalyzed p-GaP based photoelectrochemical cell," *Journal of the American Chemical Society*, vol. 130, no. 20, pp. 6342–6344, 2008.

[299] T. Sakakura, J.-C. Choi, and H. Yasuda, "Transformation of carbon dioxide," *Chemical Reviews*, vol. 107, no. 6, pp. 2365–2387, 2007.

[300] A. J. Morris, G. J. Meyer, and E. Fujita, "Molecular approaches to the photocatalytic reduction of carbon dioxide for solar fuels," *Accounts of Chemical Research*, vol. 42, no. 12, pp. 1983–1994, 2009.

[301] H. Takeda and O. Ishitani, "Development of efficient photocatalytic systems for CO_2 reduction using mononuclear and multinuclear metal complexes based on mechanistic studies," *Coordination Chemistry Reviews*, vol. 254, no. 3-4, pp. 346–354, 2010.

[302] I. Taniguchi, B. Aurian-Blajeni, and J. O. M. Bockris, "The reduction of carbon dioxide at illuminated p-type semiconductor electrodes in nonaqueous media," *Electrochimica Acta*, vol. 29, no. 7, pp. 923–932, 1984.

[303] R. Hinogami, Y. Nakamura, S. Yae, and Y. Nakato, "An approach to ideal semiconductor electrodes for efficient photoelectrochemical reduction of carbon dioxide by modification with small metal particles," *Journal of Physical Chemistry B*, vol. 102, no. 6, pp. 974–980, 1998.

[304] J. Zheng, T. Lu, T. M. Cotton, and G. Chumanov, "Photoelectrochemical reduction of CO_2 mediated with methylviologen at roughened silver electrodes," *Journal of Electroanalytical Chemistry*, vol. 518, no. 1, pp. 6–12, 2002.

[305] R. Zhou and M. I. Guzman, "CO_2 reduction under periodic illumination of ZnS," *The Journal of Physical Chemistry C*, vol. 118, no. 22, pp. 11649–11656, 2014.

[306] M. R. Singh, E. L. Clark, and A. T. Bell, "Effects of electrolyte, catalyst, and membrane composition and operating conditions on the performance of solar-driven electrochemical reduction of carbon dioxide," *Physical Chemistry Chemical Physics*, vol. 17, no. 29, pp. 18924–18936, 2015.

[307] A. B. Bocarsly, Q. D. Gibson, A. J. Morris et al., "Comparative study of imidazole and pyridine catalyzed reduction of carbon dioxide at illuminated iron pyrite electrodes," *ACS Catalysis*, vol. 2, no. 8, pp. 1684–1692, 2012.

[308] K. Rajeshwar, N. R. de Tacconi, G. Ghadimkhani, W. Chanmanee, and C. Janáky, "Tailoring copper oxide semiconductor nanorod arrays for photoelectrochemical reduction of carbon dioxide to methanol," *ChemPhysChem*, vol. 14, no. 10, pp. 2251–2259, 2013.

[309] G. Adam, F. Aslan, E. Portenkirchner, P. Stadler, M. C. Scharber, and N. S. Sariciftci, "Electrocatalytic reduction of carbon dioxide using Sol-gel processed Copper Indium Sulfide (CIS) immobilized on ITO-coated glass electrode," *Electrocatalysis*, vol. 6, no. 4, pp. 405–413, 2015.

[310] R. Schrebler, P. Cury, F. Herrera, H. Gómez, and R. Córdova, "Study of the electrochemical reduction of CO_2 on electrodeposited rhenium electrodes in methanol media," *Journal of Electroanalytical Chemistry*, vol. 516, no. 1-2, pp. 23–30, 2001.

[311] G. Magesh, E. S. Kim, H. J. Kang et al., "A versatile photoanode-driven photoelectrochemical system for conversion of CO_2 to fuels with high faradaic efficiencies at low bias potentials," *Journal of Materials Chemistry A*, vol. 2, no. 7, pp. 2044–2049, 2014.

[312] I. Mora-Seró, T. Dittrich, G. Garcia-Belmonte, and J. Bisquert, "Determination of spatial charge separation of diffusing

electrons by transient photovoltage measurements," *Journal of Applied Physics*, vol. 100, no. 10, Article ID 103705, 6 pages, 2006.

[313] H. J. Mandujano-Ramírez, J. P. González-Vázquez, G. Oskam et al., "Charge separation at disordered semiconductor heterojunctions from random walk numerical simulations," *Physical Chemistry Chemical Physics*, vol. 16, no. 9, pp. 4082–4091, 2014.

[314] E. A. Gibson, M. Awais, D. Dini et al., "Dye sensitised solar cells with nickel oxide photocathodes prepared via scalable microwave sintering," *Physical Chemistry Chemical Physics*, vol. 15, no. 7, pp. 2411–2420, 2013.

[315] J. Bisquert, A. Zaban, and P. Salvador, "Analysis of the mechanisms of electron recombination in nanoporous TiO_2 dye-sensitized solar cells. Nonequilibrium steady-state statistics and interfacial electron transfer via surface states," *Journal of Physical Chemistry B*, vol. 106, no. 34, pp. 8774–8782, 2002.

[316] I. Mora-Seró, T. Dittrich, A. Belaidi, G. Garcia-Belmonte, and J. Bisquert, "Observation of diffusion and tunneling recombination of dye-photoinjected electrons in ultrathin TiO_2 layers by surface photovoltage transients," *The Journal of Physical Chemistry B*, vol. 109, no. 31, pp. 14932–14938, 2005.

[317] T. J. Macdonald, Y. J. Mange, M. R. Dewi et al., "$CuInS_2$/ZnS nanocrystals as sensitisers for NiO photocathodes," *Journal of Materials Chemistry A*, vol. 3, no. 25, pp. 13324–13331, 2015.

[318] J. Chen, L. Zhang, Z. Lam et al., "Tunneling interlayer for efficient transport of charges in metal oxide electrodes," *Journal of the American Chemical Society*, vol. 138, no. 9, pp. 3183–3189, 2016.

[319] B. Liu and E. S. Aydil, "Growth of oriented single-crystalline rutile TiO_2 nanorods on transparent conducting substrates for dye-sensitized solar cells," *Journal of the American Chemical Society*, vol. 131, no. 11, pp. 3985–3990, 2009.

[320] J. Bisquert and V. S. Vikhrenko, "Interpretation of the time constants measured by kinetic techniques in nanostructured semiconductor electrodes and dye-sensitized solar cells," *Journal of Physical Chemistry B*, vol. 108, no. 7, pp. 2313–2322, 2004.

[321] M. Awais, M. Rahman, J. M. D. MacElroy, D. Dini, J. G. Vos, and D. P. Dowling, "Application of a novel microwave plasma treatment for the sintering of nickel oxide coatings for use in dye-sensitized solar cells," *Surface and Coatings Technology*, vol. 205, no. 2, pp. S245–S249, 2011.

[322] J. Bisquert, D. Cahen, G. Hodes, S. Rühle, and A. Zaban, "Physical chemical principles of photovoltaic conversion with nanoparticulate, mesoporous dye-sensitized solar cells," *The Journal of Physical Chemistry B*, vol. 108, no. 24, pp. 8106–8118, 2004.

[323] S. Sumikura, S. Mori, S. Shimizu, H. Usami, and E. Suzuki, "Syntheses of NiO nanoporous films using nonionic triblock copolymer templates and their application to photo-cathodes of p-type dye-sensitized solar cells," *Journal of Photochemistry and Photobiology A: Chemistry*, vol. 199, no. 1, pp. 1–7, 2008.

[324] X. L. Zhang, F. Huang, A. Nattestad et al., "Enhanced open-circuit voltage of p-type DSC with highly crystalline NiO nanoparticles," *Chemical Communications*, vol. 47, no. 16, pp. 4808–4810, 2011.

[325] G. Boschloo and A. Hagfeldt, "Spectroelectrochemistry of nanostructured NiO," *The Journal of Physical Chemistry B*, vol. 105, no. 15, pp. 3039–3044, 2001.

[326] M. Bonomo and D. Dini, "Nanostructured p-type semiconductor electrodes and photoelectrochemistry of their reduction processes," *Energies*, vol. 9, no. 5, p. 373, 2016.

[327] S. Powar, Q. Wu, M. Weidelener et al., "Improved photocurrents for p-type dye-sensitized solar cells using nano-structured nickel(II) oxide microballs," *Energy & Environmental Science*, vol. 5, no. 10, pp. 8896–8900, 2012.

[328] I. Venditti, N. Barbero, M. V. Russo et al., "Electrodeposited ZnO with squaraine sentisizers as photoactive anode of DSCs," *Materials Research Express*, vol. 1, no. 1, Article ID 015040, 18 pages, 2014.

[329] C.-P. Lee, R. Y.-Y. Lin, L.-Y. Lin et al., "Recent progress in organic sensitizers for dye-sensitized solar cells," *RSC Advances*, vol. 5, no. 30, pp. 23810–23825, 2015.

[330] H. Gerischer, M. E. Michel-Beyerle, F. Rebentrost, and H. Tributsch, "Sensitization of charge injection into semiconductors with large band gap," *Electrochimica Acta*, vol. 13, no. 6, pp. 1509–1515, 1968.

[331] A. Ofir, S. Dor, L. Grinis, A. Zaban, T. Dittrich, and J. Bisquert, "Porosity dependence of electron percolation in nanoporous TiO_2 layers," *Journal of Chemical Physics*, vol. 128, no. 6, Article ID 064703, pp. 1–9, 2008.

[332] A. Hagfeldt, U. B. Cappel, G. Boschloo et al., "Dye sensitized photoelectrochemical cells," in *Practical Handbook of Photovoltaics: Fundamentals and Applications*, A. McEvoy, T. Markvart, and L. Castaner, Eds., pp. 479–542, Elsevier, Amsterdam, Netherlands, 2nd edition, 2012.

[333] T. Lana-Villarreal, J. Bisquert, I. Mora-Seró, and P. Salvador, "Experimental evidence of a UV light-induced long-range electric field in nanostructured TiO_2 Thin Films in Contact with Aqueous Electrolytes," *Journal of Physical Chemistry B*, vol. 109, no. 20, pp. 10355–10361, 2005.

[334] A. Hagfeld and M. Grätzel, "Light-induced redox reactions in nanocrystalline systems," *Chemical Reviews*, vol. 95, no. 1, pp. 49–68, 1995.

[335] L. Brus, "Electronic wave functions in semiconductor clusters: experiment and theory," *The Journal of Physical Chemistry*, vol. 90, no. 12, pp. 2555–2560, 1986.

[336] J. P. Gonzalez-Vazquez, V. Morales-Flórez, and J. A. Anta, "How important is working with an ordered electrode to improve the charge collection efficiency in nanostructured solar cells?" *Journal of Physical Chemistry Letters*, vol. 3, no. 3, pp. 386–393, 2012.

[337] M. Furlan, "Electronic transport and the localization length in the quantum Hall effect," *Physical Review B—Condensed Matter and Materials Physics*, vol. 57, no. 23, pp. 14818–14828, 1998.

[338] J. Bisquert, "Hopping transport of electrons in dye-sensitized solar cells," *The Journal of Physical Chemistry C*, vol. 111, no. 46, pp. 17163–17168, 2007.

[339] J. P. Gonzalez-Vazquez, J. A. Anta, and J. Bisquert, "Random walk numerical simulation for hopping transport at finite carrier concentrations: diffusion coefficient and transport energy concept," *Physical Chemistry Chemical Physics*, vol. 11, no. 44, pp. 10359–10367, 2009.

[340] U. Nandi, D. Jana, and D. Talukdar, "Scaling description of non-ohmic direct current conduction in disordered systems," *Progress in Materials Science*, vol. 71, pp. 1–92, 2015.

[341] J. Bisquert and A. Zaban, "The trap-limited diffusivity of electrons in nanoporous semiconductor networks permeated with a conductive phase," *Applied Physics A*, vol. 77, no. 3-4, pp. 507–514, 2003.

[342] J. Bisquert, "Chemical diffusion coefficient of electrons in nanostructured semiconductor electrodes and dye-sensitized solar cells," *Journal of Physical Chemistry B*, vol. 108, no. 7, pp. 2323–2332, 2004.

[343] T. Dittrich, I. Mora-Seró, G. García-Belmonte, and J. Bisquert, "Temperature dependent normal and anomalous electron diffusion in porous TiO_2 studied by transient surface photovoltage," *Physical Review B*, vol. 73, no. 4, Article ID 045407, pp. 1–8, 2006.

[344] J. A. Anta, I. Mora-Seró, T. Dittrich, and J. Bisquert, "Interpretation of diffusion coefficients in nanostructured materials from random walk numerical simulation," *Physical Chemistry Chemical Physics*, vol. 10, no. 30, pp. 4478–4485, 2008.

[345] J. Bisquert, I. Mora-Sero, and F. Fabregat-Santiago, "Diffusion-recombination impedance model for solar cells with disorder and nonlinear recombination," *ChemElectroChem*, vol. 1, no. 1, pp. 289–296, 2014.

[346] Y. Zhao and K. Zhu, "Organic-inorganic hybrid lead halide perovskites for optoelectronic and electronic applications," *Chemical Society Reviews*, vol. 45, no. 3, pp. 655–689, 2016.

[347] S. Ye, W. Sun, Y. Li et al., "CuSCN-based inverted planar perovskite solar cell with an average PCE of 15.6%," *Nano Letters*, vol. 15, no. 6, pp. 3723–3728, 2015.

[348] X. Yin, P. Chen, M. Que et al., "Highly efficient flexible perovskite solar cells using solution-derived NiO_x hole contacts," *ACS Nano*, vol. 10, no. 3, pp. 3630–3636, 2016.

[349] K.-C. Wang, J.-Y. Jeng, P.-S. Shen et al., "P-type mesoscopic nickel oxide/organometallic perovskite heterojunction solar cells," *Scientific Reports*, vol. 4, pp. 4756–4763, 2014.

[350] J. H. Park, J. Seo, S. Park et al., "Efficient $CH_3NH_3PbI_3$ perovskite solar cells employing nanostructured p–type NiO electrode formed by a pulsed laser deposition," *Advanced Materials*, vol. 27, no. 27, pp. 4013–4019, 2015.

[351] W. Chen, Y. Wu, J. Liu et al., "Hybrid interfacial layer leads to solid performance improvement of inverted perovskite solar cells," *Energy and Environmental Science*, vol. 8, no. 2, pp. 629–640, 2015.

[352] H. Zhang, J. Cheng, F. Lin et al., "Pinhole-free and surface-nanostructured NiO_x film by room-temperature solution process for high-performance flexible perovskite solar cells with good stability and reproducibility," *ACS Nano*, vol. 10, no. 1, pp. 1503–1511, 2016.

[353] M.-H. Li, P.-S. Shen, K.-C. Wang, T.-F. Guo, and P. Chen, "Inorganic p-type contact materials for perovskite-based solar cells," *Journal of Materials Chemistry A*, vol. 3, no. 17, pp. 9011–9019, 2015.

[354] K.-C. Wang, P.-S. Shen, M.-H. Li et al., "Low-temperature sputtered nickel oxide compact thin film as effective electron blocking layer for mesoscopic $NiO/CH_3NH_3PbI_3$ perovskite heterojunction solar cells," *ACS Applied Materials and Interfaces*, vol. 6, no. 15, pp. 11851–11858, 2014.

[355] J. H. Kim, P.-W. Liang, S. T. Williams et al., "High-performance and environmentally stable planar heterojunction perovskite solar cells based on a solution-processed copper-doped nickel oxide hole-transporting layer," *Advanced Materials*, vol. 27, no. 4, pp. 695–701, 2015.

[356] J.-Y. Jeng, K.-C. Chen, T.-Y. Chiang et al., "Nickel oxide electrode interlayer in $CH_3NH_3PbI_3$ perovskite/PCBM planar-heterojunction hybrid solar cells," *Advanced Materials*, vol. 26, no. 24, pp. 4107–4113, 2014.

[357] Z. Zhu, Y. Bai, T. Zhang et al., "High-performance hole-extraction layer of sol-gel-processed NiO nanocrystals for inverted planar perovskite solar cells," *Angewandte Chemie International Edition*, vol. 53, no. 46, pp. 12571–12575, 2014.

[358] H. Tian, B. Xu, H. Chen, E. M. J. Johansson, and G. Boschloo, "Solid-state perovskite-sensitized p-type mesoporous nickel oxide solar cells," *ChemSusChem*, vol. 7, no. 8, pp. 2150–2153, 2014.

[359] Z. Liu, M. Zhang, X. Xu et al., "NiO nanosheets as efficient top hole transporters for carbon counter electrode based perovskite solar cells," *Journal of Materials Chemistry A*, vol. 3, no. 47, pp. 24121–24127, 2015.

[360] V. Trifiletti, V. Roiati, S. Colella et al., "$NiO/MAPbI_{3-x}Cl_x$/PCBM: a model case for an improved understanding of inverted mesoscopic solar cells," *ACS Applied Material Interfaces*, vol. 7, no. 7, pp. 4283–4289, 2015.

[361] Z. Liu, M. Zhang, X. Xu et al., "P-Type mesoscopic NiO as an active interfacial layer for carbon counter electrode based perovskite solar cells," *Dalton Transactions*, vol. 44, no. 9, pp. 3967–3973, 2015.

[362] W. Chen, Y. Wu, Y. Yue et al., "Efficient and stable large-area perovskite solar cells with inorganic charge extraction layers," *Science*, vol. 350, no. 6263, pp. 944–948, 2015.

[363] H. Rao, W. Sun, S. Ye et al., "Solution-processed CuS NPs as an inorganic hole-selective contact material for inverted planar perovskite solar cells," *ACS Applied Materials & Interfaces*, vol. 8, no. 12, pp. 7800–7805, 2016.

[364] X. Yin, M. Que, Y. Xing, and W. Que, "High efficiency hysteresis-less inverted planar heterojunction perovskite solar cells with a solution-derived NiO_x hole contact layer," *Journal of Material Chemistry A*, vol. 3, no. 48, pp. 4495–24503, 2015.

[365] W.-Y. Chen, L.-L. Deng, S.-M. Dai et al., "Low-cost solution-processed copper iodide as an alternative to PEDOT:PSS hole transport layer for efficient and stable inverted planar heterojunction perovskite solar cells," *Journal of Materials Chemistry A*, vol. 3, no. 38, pp. 19353–19359, 2015.

[366] J. Cui, F. Meng, H. Zhang et al., "$CH_3NH_3PbI_3$-based planar solar cells with magnetron-sputtered nickel oxide," *ACS Applied Materials & Interfaces*, vol. 6, no. 24, pp. 22862–22870, 2014.

[367] L. Hu, J. Peng, W. W. Wang et al., "Sequential deposition of $CH_3NH_3PbI_3$ on planar NiO film for efficient planar perovskite solar cells," *ACS Photonics*, vol. 1, no. 7, pp. 547–553, 2014.

[368] S. Chatterjee and A. J. Pal, "Introducing Cu_2O thin films as a hole-transport layer in efficient planar perovskite solar cell structures," *Journal of Physical Chemistry C*, vol. 120, no. 3, pp. 1428–1437, 2016.

[369] J. W. Jung, C.-C. Chueh, and A. K.-Y. Jen, "A low-temperature, solution-processable, cu-doped nickel oxide hole-transporting layer via the combustion method for high-performance thin-film perovskite solar cells," *Advanced Materials*, vol. 27, no. 47, pp. 7874–7880, 2015.

[370] K. Zhao, R. Munir, B. Yan, Y. Yang, T. Kim, and A. Amassian, "Solution-processed inorganic copper(i) thiocyanate (CuSCN) hole transporting layers for efficient p-i-n perovskite solar cells," *Journal of Materials Chemistry A*, vol. 3, no. 41, pp. 20554–20559, 2015.

[371] B. Abdollahi Nejand, V. Ahmadi, and H. R. Shahverdi, "New physical deposition approach for low cost inorganic hole transport layer in normal architecture of durable perovskite solar cells," *ACS Applied Materials and Interfaces*, vol. 7, no. 39, pp. 21807–21818, 2015.

[372] J. You, L. Meng, T.-B. Song et al., "Improved air stability of perovskite solar cells via solution-processed metal oxide transport layers," *Nature Nanotechnology*, vol. 11, no. 1, pp. 75–81, 2016.

[373] X. Xu, Z. Liu, Z. Zuo et al., "Hole selective NiO contact for efficient perovskite solar cells with carbon electrode," *Nano Letters*, vol. 15, no. 4, pp. 2402–2408, 2015.

[374] P. Docampo, J. M. Ball, M. Darwich, G. E. Eperon, and H. J. Snaith, "Efficient organometal trihalide perovskite planar-heterojunction solar cells on flexible polymer substrates," *Nature Communications*, vol. 4, article 2761, 6 pages, 2013.

[375] W.-C. Lai, K.-W. Lin, T.-F. Guo, and J. Lee, "Perovskite-based solar cells with nickel-oxidized nickel oxide hole transfer layer," *IEEE Transactions on Electron Devices*, vol. 62, no. 5, pp. 1590–1595, 2015.

[376] C. Zuo and L. Ding, "Solution-processed Cu_2O and CuO as hole transport materials for efficient perovskite solar cells," *Small*, vol. 11, no. 41, pp. 5528–5532, 2015.

[377] M. I. Hossain, F. H. Alharbi, and N. Tabet, "Copper oxide as inorganic hole transport material for lead halide perovskite based solar cells," *Solar Energy*, vol. 120, pp. 370–380, 2015.

[378] S. Ito, S. Tanaka, H. Vahlman, H. Nishino, K. Manabe, and P. Lund, "Carbon-double-bond-free printed solar cells from $TiO_2/CH_3NH_3PbI_3$/CuSCN/Au: structural control and photoaging effects," *ChemPhysChem*, vol. 15, no. 6, pp. 1194–1200, 2014.

[379] A. S. Subbiah, A. Halder, S. Ghosh, N. Mahuli, G. Hodes, and S. K. Sarkar, "Inorganic hole conducting layers for perovskite-based solar cells," *Journal of Physical Chemistry Letters*, vol. 5, no. 10, pp. 1748–1753, 2014.

[380] P. Qin, S. Tanaka, S. Ito et al., "Inorganic hole conductor-based lead halide perovskite solar cells with 12.4% conversion efficiency," *Nature Communications*, vol. 5, article 3834, 6 pages, 2014.

[381] J. Shi, X. Xu, D. Li, and Q. Meng, "Interfaces in perovskite solar cells," *Small*, vol. 11, no. 21, pp. 2472–2486, 2015.

[382] I. J. Park, M. A. Park, D. H. Kim et al., "New hybrid hole extraction layer of perovskite solar cells with a planar p–i–n geometry," *The Journal of Physical Chemistry C*, vol. 119, no. 49, pp. 27285–27290, 2015.

[383] L. Meng, J. B. You, T.-F. Guo, and Y. Yang, "Recent advances in the inverted planar structure of perovskite solar cells," *Accounts of Chemical Research*, vol. 49, no. 1, pp. 155–165, 2016.

[384] I. R. Perera, T. Daeneke, S. Makuta et al., "Application of the tris(acetylacetonato)iron(III)/(II) redox couple in p-type dye-sensitized solar cells," *Angewandte Chemie—International Edition*, vol. 54, no. 12, pp. 3758–3762, 2015.

[385] S. Powar, T. Daeneke, M. T. Ma et al., "Highly efficient p-type dye-sensitized solar cells based on tris(1,2-diaminoethane)cobalt(II)/(III) electrolytes," *Angewandte Chemie—International Edition*, vol. 52, no. 2, pp. 602–605, 2013.

[386] A. Yella, H. W. Lee, H. N. Tsao et al., "Porphyrin-sensitized solar cells with cobalt (II/III)-based redox electrolyte exceed 12 percent efficiency," *Science*, vol. 334, no. 6053, pp. 629–634, 2011.

[387] K. Kakiage, Y. Aoyama, T. Yano, K. Oya, J.-I. Fujisawa, and M. Hanaya, "Highly-efficient dye-sensitized solar cells with collaborative sensitization by silyl-anchor and carboxy-anchor dyes," *Chemical Communications*, vol. 51, no. 88, pp. 15894–15897, 2015.

[388] T. Daeneke, T.-H. Kwon, A. B. Holmes, N. W. Duffy, U. Bach, and L. Spiccia, "High-efficiency dye-sensitized solar cells with ferrocene-based electrolytes," *Nature Chemistry*, vol. 3, no. 3, pp. 211–215, 2011.

[389] W. Shockley and H. J. Queisser, "Detailed balance limit of efficiency of p-n junction solar cells," *Journal of Applied Physics*, vol. 32, no. 3, pp. 510–519, 1961.

[390] C. J. Wood, K. C. D. Robson, P. I. P. Elliott, C. P. Berlinguette, and E. A. Gibson, "Novel triphenylamine-modified ruthenium(II) terpyridine complexes for nickel oxide-based cathodic dye-sensitized solar cells," *RSC Advances*, vol. 4, no. 11, pp. 5782–5791, 2014.

[391] J.-F. Lefebvre, X.-Z. Sun, J. A. Calladine, M. W. George, and E. A. Gibson, "Promoting charge-separation in p-type dye-sensitized solar cells using bodipy," *Chemical Communications*, vol. 50, no. 40, pp. 5258–5260, 2014.

[392] X. L. Zhang, Z. Zhang, F. Huang, P. Bäuerle, U. Bach, and Y.-B. Cheng, "Charge transport in photocathodes based on the sensitization of NiO nanorods," *Journal of Materials Chemistry*, vol. 22, no. 14, pp. 7005–7009, 2012.

[393] L. Le Pleux, A. L. Smeigh, E. Gibson et al., "Synthesis, photophysical and photovoltaic investigations of acceptor-functionalized perylene monoimide dyes for nickel oxide p-type dye-sensitized solar cells," *Energy and Environmental Science*, vol. 4, no. 6, pp. 2075–2084, 2011.

[394] A. Nattestad, X. Zhang, U. Bach, and Y.-B. Cheng, "Dye-sensitized $CuAlO_2$ photocathodes for tandem solar cell applications," *Journal of Photonics for Energy*, vol. 1, no. 1, Article ID 11103, 2011.

[395] A. Renaud, B. Chavillon, L. Le Pleux et al., "$CuGaO_2$: a promising alternative for NiO in p-type dye solar cells," *Journal of Materials Chemistry*, vol. 22, no. 29, pp. 14353–14356, 2012.

[396] D. Xiong, Z. Xu, X. Zeng et al., "Hydrothermal synthesis of ultrasmall $CuCrO_2$ nanocrystal alternatives to NiO nanoparticles in efficient p-type dye-sensitized solar cells," *Journal of Materials Chemistry*, vol. 22, no. 47, pp. 24760–24768, 2012.

[397] Z. Xu, D. Xiong, H. Wang et al., "Remarkable photocurrent of p-type dye-sensitized solar cell achieved by size controlled $CuGaO_2$ nanoplates," *Journal of Materials Chemistry A*, vol. 2, no. 9, pp. 2968–2976, 2014.

[398] M. Yu, G. Natu, Z. Ji, and Y. Wu, "P-type dye-sensitized solar cells based on delafossite $CuGaO_2$ nanoplates with saturation photovoltages exceeding 460 mV," *Journal of Physical Chemistry Letters*, vol. 3, no. 9, pp. 1074–1078, 2012.

[399] S. Powar, R. Bhargava, T. Daeneke et al., "Thiolate/disulfide based electrolytes for p-type and tandem dye-sensitized solar cells," *Electrochimica Acta*, vol. 182, pp. 458–463, 2015.

[400] X. Xu, B. Zhang, J. Cui et al., "Efficient p-type dye-sensitized solar cells based on disulfide/thiolate electrolytes," *Nanoscale*, vol. 5, no. 17, pp. 7963–7969, 2013.

[401] E. Sheibani, L. Zhang, P. Liu et al., "A study of oligothiophene-acceptor dyes in p-type dye-sensitized solar cells," *RSC Advances*, vol. 6, no. 22, pp. 18165–18177, 2016.

[402] F. Wu, L. Zhu, S. Zhao, Q. Song, and C. Yang, "Engineering of organic dyes for highly efficient p-type dye-sensitized solar cells," *Dyes and Pigments*, vol. 124, pp. 93–100, 2016.

[403] S. Powar, D. Xiong, T. Daeneke et al., "Improved photovoltages for p-type dye-sensitized solar cells using $CuCrO_2$ nanoparticles," *Journal of Physical Chemistry C*, vol. 118, no. 30, pp. 16375–16379, 2014.

[404] J. Cui, J. Lu, X. Xu et al., "Organic sensitizers with pyridine ring anchoring group for p-type dye-sensitized solar cells," *The Journal of Physical Chemistry C*, vol. 118, no. 30, pp. 16433–16440, 2014.

[405] K. A. Click, D. R. Beauchamp, B. R. Garrett, Z. Huang, C. M. Hadad, and Y. Wu, "A double-acceptor as a superior organic dye design for p-type DSSCs: high photocurrents and the observed light soaking effect," *Physical Chemistry Chemical Physics*, vol. 16, no. 47, pp. 26103–26111, 2014.

[406] Q.-Q. Zhang, K.-J. Jiang, J.-H. Huang et al., "A push-pull thienoquinoidal chromophore for highly efficient p-type dye-sensitized solar cells," *Journal of Materials Chemistry A*, vol. 3, no. 15, pp. 7695–7698, 2015.

[407] X. Xu, J. Cui, J. Han et al., "Near field enhanced photocurrent generation in P-type dye-sensitized solar cells," *Scientific Reports*, vol. 4, article 3961, 2014.

[408] L. Zhang, G. Boschloo, L. Hammarström, and H. Tian, "Solid state p-type dye-sensitized solar cells: concept, experiment and mechanism," *Physical Chemistry Chemical Physics*, vol. 18, no. 7, pp. 5080–5085, 2016.

[409] J. Qian, K.-J. Jiang, J.-H. Huang, Q.-S. Liu, L.-M. Yang, and Y. Song, "A selenium-based cathode for a high-voltage tandem photoelectrochemical solar cell," *Angewandte Chemie—International Edition*, vol. 51, no. 41, pp. 10351–10354, 2012.